Geophys. J. Int. (1990) **102,** 695–731

Earthquake mechanisms in the Hellenic Trench near Crete

T. Taymaz,[1] J. Jackson[1] and R. Westaway[2]
[1]*Department of Earth Sciences, Bullard Laboratories, Madingley Road, Cambridge* CB3 0EZ, *UK*
[2]*Department of Geological Sciences, South Road, Durham* DH1 3LE, *UK*

Accepted 1990 April 6. Received 1990 April 6; in original form 1989 December 28

SUMMARY

In the Hellenic Trench south of Crete convergence between the southern Aegean Sea and Africa occurs at a rate of at least 60 mm yr^{-1}. Previously published first motion fault plane solutions show a variety of different fault orientations and types, but are not well constrained. Furthermore, the lack of reliable focal depths for these earthquakes has obscured any simple pattern of deformation that might exist. Nonetheless, the mechanisms of these earthquakes have strongly influenced views of the tectonics in the Hellenic Trench. We have improved estimates of the fault parameters and focal depths for 14 of these earthquakes, using long-period *P*- and *SH*-waveforms. The earthquake mechanisms fall into four groups: **(a)** normal faults with a N–S strike in the over-riding material above the subduction zone; **(b)** low-angle thrusts with an E–W strike at a depth of about 40 km; **(c)** high-angle reverse faults with the same strike but shallower focal depths than (b); **(d)** events within the suducting lithosphere with approximately E–W *P* axes. The thrusting in groups (b) and (c) is probably the mechanism by which the sediments of the Mediterranean Sea underplate and uplift Crete. These events have slip vectors in the direction $025 \pm 12°$ which represents the convergence direction between Crete and Africa along the SW-facing boundary of the Hellenic Trench. One of the events in group (d) occurred beneath the Mediterranean Ridge and involved high-angle reverse faulting with a WNW–ESE *P* axis: almost perpendicular to the direction of shortening deduced from folds at the surface. The Mediterranean Sea floor in this region appears to be in a state of E–W compression, for reasons that are not clear.

Key words: Crete, earthquakes, faulting, Hellenic Trench, Mediterranean, subduction.

1 INTRODUCTION

This paper is concerned with the geometry of faulting in the Hellenic arc near Crete (Fig. 1), and is based on observations of earthquake focal mechanisms and depths. The region is one of intense seismicity, most of which occurs in a belt about 100 km wide that roughly follows the bathymetric expression of the Hellenic Trench (McKenzie 1978). Fault plane solutions of the larger earthquakes show mainly thrust faulting (McKenzie 1972, 1978; Ritsema 1974), and indicate shortening between Crete and the Mediterranean Sea floor further south. Earthquakes occur to depths of about 150–180 km in an irregular zone that dips to the north (e.g. Papazachos 1973; Comninakis & Papazachos 1980; Martin 1988) and presumably identifies a subducted lithosphere slab. North of the Hellenic Trench lies the Aegean extensional province, which has been stretched and thinned by normal faulting (McKenzie 1978; Le Pichon & Angelier 1979). Within the extensional province, the seismicity is most intense in the northern Aegean and coastal regions of Greece and western Turkey: the Sea of Crete and the Cyclades are relatively aseismic, though studies on land and at sea reveal Neogene normal faulting that continues as far south as the inner wall of the Hellenic Trench (Angelier *et al.* 1982; Huchon *et al.* 1982).

The seismicity in the region of Crete is thus related to both the north–south convergence between Africa and Europe, known to be about 10 mm yr^{-1} (Chase 1978), and the extension within the Aegean province. Various estimates have been made of the present rate of extension in the Aegean, based on either kinematic arguments (McKenzie 1978; Le Pichon & Angelier 1979), seismic moment rates (Jackson & McKenzie 1988a, b; Ekstrom & England 1989; Main & Burton 1989), or, more recently by direct measurement using satellite laser-ranging (Sellers & Cross 1989). All are agreed that the north–south extension

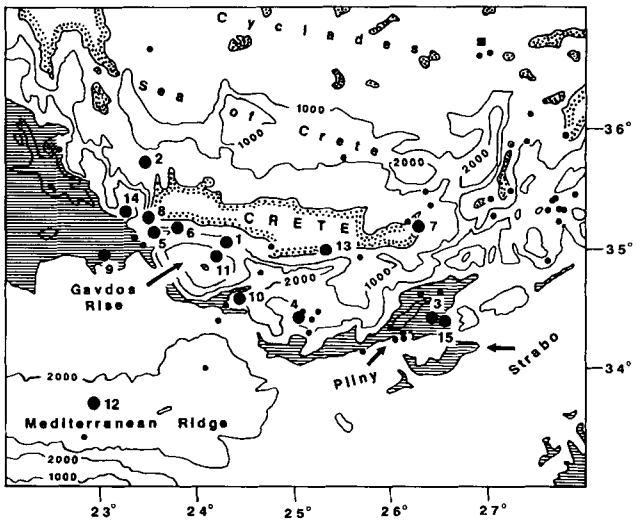

Figure 1. Bathymetric map of the region around Crete. Contours are at intervals of 1000 m, and shaded below 3000 m, taken from the IOC–UNESCO (1981) 1:1 000 000 bathymetric map of the Mediterranean. Filled circles are ISC epicentres for 1961–1988. Large symbols are those of earthquakes discussed in this paper: adjacent numbers refer to events in Tables 1–3. Smaller symbols are for events of $m_b > 5.0$. The filled square in the NE corner is the epicentre of the only event of $m_b > 5.0$ whose depth (159 km) exceeds 150 km.

rate across the Aegean is considerably faster than the convergence between Africa and Europe. Likely extension rates are in the range 40–60 mm yr^{-1}, with accompanying shortening in the Hellenic Trench of at least 50–60 mm yr^{-1}. However, while the seismicity can account for most of the expected motion in the extensional province, it is clear that there are not nearly enough earthquakes in the Hellenic Trench to account for the shortening there: as much as 90 per cent of it may be occurring aseismically (see Jackson & McKenzie 1988b for a review).

The length of time over which these present-day rates of extension and convergence have been operating is not clear. The length of the seismically active part of the subducting slab is about 300 km, all of which could have been thrust into the mantle within the last 5 Myr at the present-day convergence rates. The present-day rates could also have produced most of the observed extensional strain in the Aegean within the last 5 Myr (Jackson & McKenzie 1988b), though there is no doubt that the strain has varied spatially over that time (e.g. Mercier *et al.* 1989). Geological arguments for the duration of stretching and subduction are controversial. Extensional structures are seen in Greece in Miocene time, though Mercier *et al.* (1989) argue that most of the extensional strain occurred in the last 5 Myr. This opinion is shared by Kissel & Laj (1988), who link the large (about 25°) post-5 Myr clockwise rotation of the western Peloponnese relative to Europe to the onset of extension in the Aegean. The onset of subduction is even more loosely constrained. Le Pichon & Angelier (1979) suggest the subduction started about 13 Myr ago, based on the age of the oldest volcanic rocks associated with the arc (2.7 Myr) and an assumption about the shape of the sinking slab. Mercier *et al.* (1989) date the onset of shortening in the Ionian islands to Langhian time (16 Myr), which, if it accompanied subduction of seafloor, suggests a date similar to that deduced by Le Pichon & Angelier (1979). Spakman (1986), Spakman *et al.* (1988) and Meulenkamp *et al.* (1988) have argued that the subduction is much older (26–40 Myr), based on controversial tomographic evidence for a slab-shaped velocity anomaly beneath the deepest earthquakes of the Benioff zone. They suggest that the maximum depth of earthquakes represents, not the deepest extent of the slab, but the deepest extent of material cold enough to generate earthquakes, which if the downgoing lithosphere is Mesozoic in age (Dercourt *et al.* 1986), could have been resident in the mantle for up to 15 Myr. Others, such as McKenzie (1978) and Kissel & Laj (1988), have suggested that the onset of subduction is likely to have accompanied the onset of rapid extension in the Aegean, and concluded that the subduction began 5 Myr ago. The details of these arguments are not relevant here: it is sufficient to emphasize the difficulties of reconciling the present-day convergence rate in the Hellenic Trench with a duration of subduction much longer than 5 Myr. Either the convergence rate must have increased recently, or the subduction south of Crete is not significantly older than 5 Myr.

The slip vectors of earthquakes in the Hellenic Trench are important constraints on the kinematic models of the arc proposed by McKenzie (1978) and by Le Pichon & Angelier (1979). In particular, Le Pichon & Angelier (1979) used an apparent variation in slip direction round the arc to locate a pole of rotation in the southern Adriatic Sea that described the motion between the southern Aegean and Africa. This model was later modified (Angelier *et al.* 1982) to account for the lack of observed palaeomagnetic rotation in Crete (Valente *et al.* 1982). These models used slip vectors taken from fault plane solutions of McKenzie (1978) or Ritsema (1974) that are based only on first motion polarities, and are often not well constrained. These first motion fault plane solutions are sufficient to show a variety of fault orientations and mechanisms that attest to the complex nature of the deformation around Crete, but without accurate focal depths it is unclear what is happening. We were anxious to see whether improvements in the quality of the focal mechanisms and depths of these earthquakes would clarify the pattern of deformation in this part of the arc.

Another motivation for this study was the occurrence in 1982 of an earthquake on the Mediterranean Ridge that was large enough for teleseismic waveform analysis. Since the work of Ryan *et al.* (1970), many authors have suggested that this structure is essentially an accretionary prism of material that has been scraped off the downgoing slab in the Hellenic Trench (see review by Le Pichon *et al.* 1982b). It appears that little of the thick sediment cover south of Crete contributes to the isotopic composition of the arc volcanics (Barton, Salters & Huijsmans 1983; Briqueu *et al.* 1986) and that, instead, it is either thickened in the Mediterranean Ridge or underplates Crete and is partly responsible for its uplift (e.g. Angelier *et al.* 1982). The large earthquake beneath the Mediterranean Ridge offers the opportunity to discover the nature of the faulting at depths greater than have been penetrated by existing seismic reflection profiles.

2 EARTHQUAKE SOURCE MECHANISM AND FOCAL DEPTHS

We used both *P*- and *SH*-waveforms and first motion polarities of *P*-waves to constrain earthquake source parameters. The approach we followed is that described by Molnar & Lyon-Caen (1989). We compared the shapes and amplitudes of *P*- and *SH*-waveforms recorded by stations in the distance range 30°–90°, and for which signal amplitudes were large enough, with synthetic waveforms. To determine source parameters we used McCaffrey & Abers' (1988) version of Nabelek's (1984) inversion procedure, which minimizes, in a weighted least-squares sense, the misfit between observed and synthetic seismograms (McCaffrey & Nabelek 1987; Nelson, McCaffrey & Molnar 1987; Fredrich, McCaffrey & Denham 1988). Seismograms are generated by combining direct (*P* or *S*) and reflected (*pP* and *sP*, or *sS*) phases from a point source embedded in a given velocity structure. Receiver structures are assumed to be homogeneous half-spaces. Amplitudes are adjusted for geometrical spreading, and for attenuation using Futterman's (1962) operator, with $t^* = 1$ s for *P* and $t^* = 4$ s for *SH*. As explained by Fredrich *et al.* (1988), uncertainties in t^* affect mainly source duration and seismic moment, rather than source orientation or centriod depth. Seismograms were weighted according to the azimuthal distribution of stations, such that stations clustered together were given smaller weights than those of isolated stations (McCaffrey & Abers 1988). The inversion routine then adjusts the strike, dip, rake, centroid depth and source time function, which is described by the amplitudes of a series of overlapping isoceles triangles (Nabelek 1984) whose number and duration we selected.

Our experience with the inversion routine was very similar to that of Nelson *et al.* (1987), McCaffrey (1988), Fredrich *et al.* (1988) and Molnar & Lyon-Caen (1989). We found that a point source, in which all slip occurs at the same point (the centroid) in space but not in time, was a good approximation for the size of earthquakes we studied (up to M_s 6.5): we saw no indication of systematic azimuthal variations in waveforms that might be associated with rupture propagation. The focal sphere was generally covered by observations in all azimuthal quadrants, and we found that estimates of the strike, dip rake and centroid depth were often relatively independent of each other. Thus if one parameter was fixed at a value within a few degrees or km of its value yielded by the minimum misfit of observed and synthetic seismograms, the inversion routine usually returned values for the other parameters that were close to those of the minimum misfit solution. The strikes and dips of nodal planes were in all cases consistent, within a few degrees, with virtually all first motion polarities (Fig. 2). The estimate of seismic moment clearly depended on the duration of the source time function, and to some extent on centroid depth and velocity structure. As our main interest is in source orientation and depth, we did not concern ourselves much with uncertainites in seismic moment. We estimated the lengths of the time functions by increasing the number of isoscles triangles until the amplitudes of the later ones became insignificant. The seismogram lengths we selected for inversion were sufficient to include the reflected phases *pP*, *sP* and *sS*. We examined the *P*-waves for *PcP* arrivals, where they were anticipated within the selected window, but this phase was never of significant amplitude. *ScS* presented a greater problem, and we generally truncated our inversion window for *S*-waves before the *ScS* arrival, even if this was before the reflected *sS* phase (recognizing in this case that we were losing information on focal depth). Where *ScS* arrives within the window we

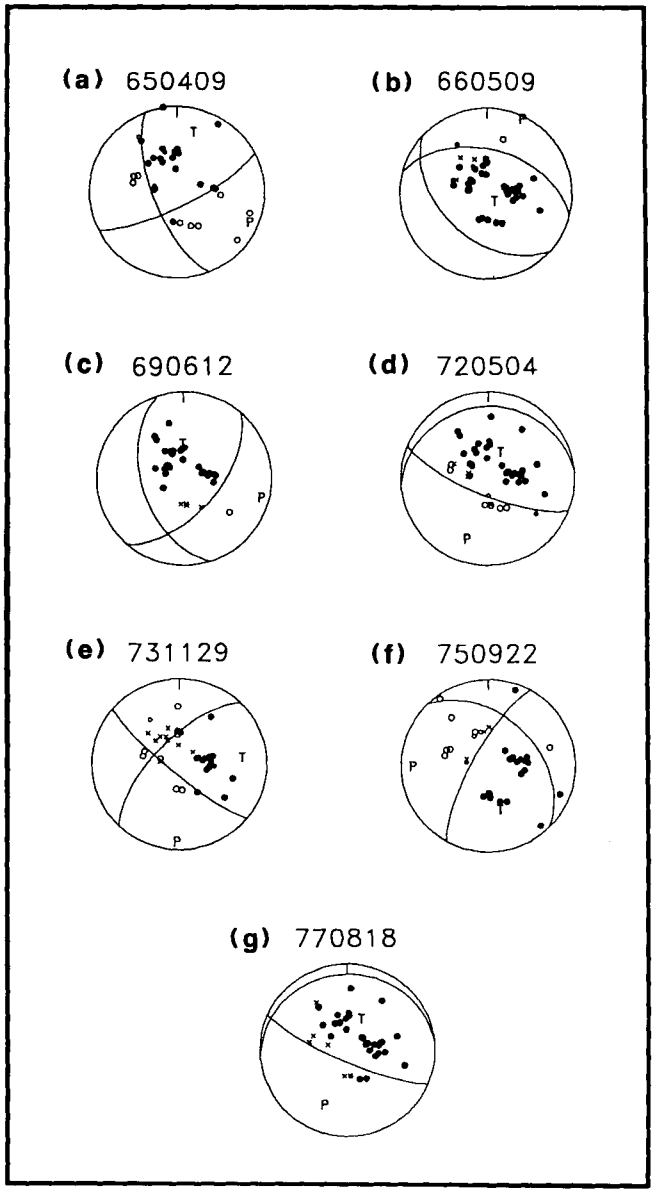

Figure 2. Lower hemisphere equal area projections of the first motion polarity data. Station positions have been plotted with the same velocity beneath the source that was used in our minimum misfit solutions. Filled circles are compressional first motions, open are dilatational. Large symbols are polarities read on long-period WWSSN instruments, small symbols are polarities based on clear short-period seismograms whose onsets display the short-period impulse response (see Jackson & McKenzie 1984). Nodal planes are those of the minimum misfit solutions. Above each sphere is the event's date (year, month, day).

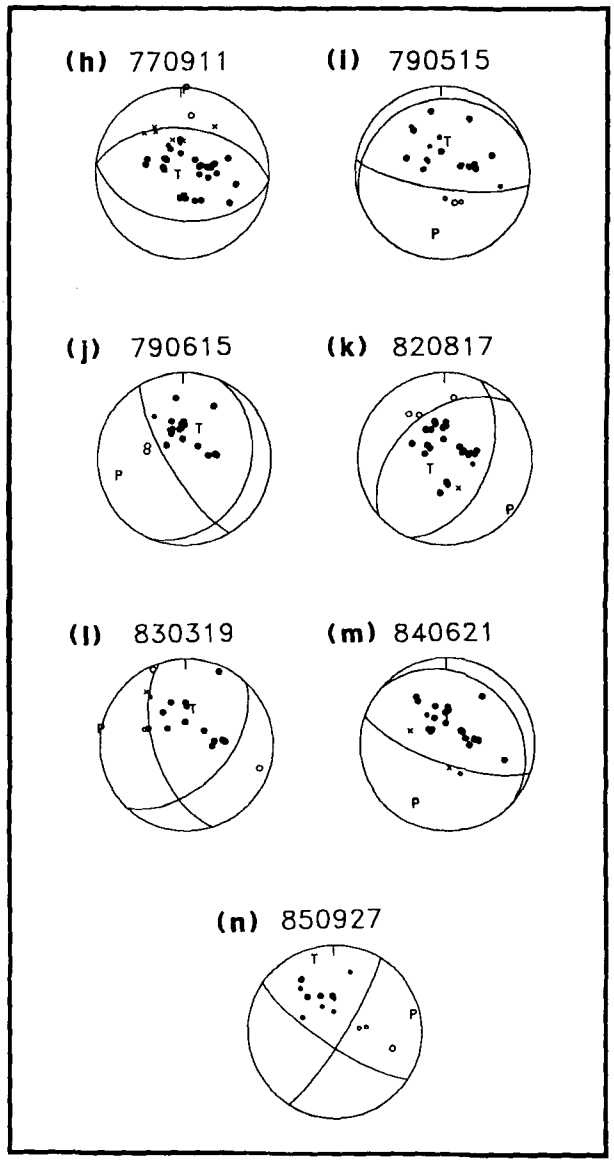

Figure 2. (*continued*)

retained, we have marked its arrival time explicitly (see, for example, COL in Fig. 3).

Uncertainties in source parameters

Having found a set of acceptable source parameters, we followed the procedure described by McCaffrey & Nabelek (1987), Nelson *et al.* (1987), Fredrich *et al.* (1988) and Molnar & Lyon-Caen (1989), in which the inversion routine is used to carry out experiments to test how well individual source parameters are resolved. We investigated one parameter at a time by fixing it at a series of values either side of its value yielded by the minimum misfit solution, and allowing the other parameters to be found by the inversion routine. We then visually examined the quality of fit between observed and synthetic seismograms to see whether it had deteriorated from the minimum misfit solution.

Although each earthquake was recorded by a different subset of stations, such that each one presented, to some extent, its own special conditions, it is possible to generalize the effects of our investigations into uncertainties in source parameters. This is because the orientations of most of the events we studied belonged to one of two groups: thrusting on roughly WNW–ESE planes or thrusting on roughly NE–SW planes. Although each earthquake is discussed in the Appendix, we will illustrate our procedure with a detailed example chosen from each group. It is necessary first to discuss velocity structure in the source region.

Source region velocity structure

The velocity structure of the crust beneath the eastern Mediterranean Sea south of Crete is imperfectly known. From an unreversed seismic refraction line on Crete, Makris (1977) estimated a mean crustal P velocity of 6.2 km s^{-1}, a Moho depth of 30–34 km, and a P_n velocity of 7.6 km s^{-1}. South and east of Crete it is clear that there is a thick (between 6 and 15 km) sedimentary cover with P velocities in the region 4.5–5.0 km s^{-1} (Makris *et al.* 1983; Makris & Stobbe 1984). Makris & Stobbe (1984) conclude, based on seismic refraction and gravity data, that the Moho is at a depth of 28–34 km beneath the Mediterranean Ridge south of Crete, where the sedimentary cover is about 10 km thick. Within the area of this study the velocity structure is likely to vary laterally, and, because of uncertainties in the ISC earthquake locations, we are not even sure whether some of the events near the south coast of Crete had epicentres on land or offshore. Our attempts to use waveform data to constrain the velocity structures in the source regions were unsuccessful: partly, we suspect, because lateral changes in the bathymetry and structure are so rapid that a single source velocity structure may be inappropriate for all recording stations (see also Nelson *et al.* 1987). Thus, for some of the events near the south coast of Crete, reflection points for *pP*, *sP* and *sS* may be on land for paths to northern stations but underwater (and through a thick sedimentary cover) for paths to other azimuths. Our approach was therefore to see how acceptable variations in source velocity structure affected our estimates of source parameters. The values of strike, dip and rake returned by the inversion routine were generally insensitive to changes in velocity structure, in that their values varied less than the uncertainties we would anyway estimate from our other tests. Not surprisingly, changes in velocity structure affected the estimates of centroid depth, because of the changes in delay time between reflected and direct phases, and of seismic moment, mainly because of changes in reflection coefficients.

The events in our study had centroid depths that were either clearly crustal (in region of 20 km) or clearly in the mantle (around 40 km or greater). For those that were clearly crustal we used a structure consisting of a layer of sediment ($V_P = 4.5$ km s^{-1}) 8 km thick above a half-space of $V_P = 6.5$ km s^{-1}; which is consistent with the results of Makris (1977), Makris *et al.* (1983) and Makris & Stobbe (1984). For those events with centroid depths in the region of 50 km or greater, we used a crust 29 km thick with an average V_P of 6.5 km s^{-1} above a mantle of $V_P = 7.8$ km s^{-1}.

We discuss an example (1972 May 4) from the group with centroid depths around 40 km in more detail below. For all

Table 1. ISC locations.

#	DATE	I. S. C. ORIGIN TIME	LAT.	LON.	DEPTH	CENTROID DEPTH	N	WATER DEPTH	VELOCITY STRUCTURE
1.	9. 4.1965	235702.0	35.060N	24.310E	39	51	210	1.0	A
*2.	27. 4.1965	140905.6	35.650N	23.530E	37	14	178		
3.	9. 5.1966	004253.0	34.430N	26.440E	13	16	206	3.0	B
4.	12. 6.1969	151331.1	34.430N	25.040E	22	19	288	3.0	B
5.	4. 5.1972	213957.0	35.150N	23.560E	14	41	332	2.0	C
6.	29.11.1973	105744.3	35.180N	23.810E	37	18	309	1.0	B
7.	22. 9.1975	004456.4	35.200N	26.260E	55	64	312	1.0	A
8.	18. 8.1977	092740.7	35.270N	23.520E	47	38	331	2.0	C
9.	11. 9.1977	231919.0	34.950N	23.050E	30	19	411	3.0	B
10.	15. 5.1979	065922.6	34.580N	24.450E	43	35	392	1.5	C
11.	15. 6.1979	113416.7	34.940N	24.210E	41	40	310	2.0	C
12.	17. 8.1982	222220.0	33.710N	22.940E	35	39	506	1.5	C
13.	19. 3.1983	214142.0	35.020N	25.320E	59	67	462	---	A
14.	21. 6.1984	104340.5	35.310N	23.280E	25	39	543	2.0	C
15.	27. 9.1985	163946.4	34.400N	26.550E	41	38	447	2.0	C

VELOCITY STRUCTURES:	Vp(kms-1)	Vs(kms-1)	Density(kgm-3)	Thickness(km)
A:	6.50	3.70	2800	24
	7.80	4.50	3300	half-space
B:	4.50	2.59	2420	8
	6.50	3.70	2800	half-space
C:	4.50	2.59	2420	8
	6.80	3.91	2910	half-space

* After Lyon-Caen et al.(1988).

apparently offshore earthquakes we included a water layer with a depth appropriate to their ISC epicentres. The water depths we used varied between 1.0 and 3.0 km, and the match between observed and synthetic seismograms did not seem to be affected in any systematic way by changes in the depth of the water layer: probably because reflected rays travelled through different water depths to different azimuths. The velocity structures we used are given in Table 1.

The earthquake of 1972 May 4

We discuss this event in detail because it belongs to the group that involved thrust faulting on roughly WNW–ESE planes, and because it was one of the events with a centroid depth around 40 km. Fig. 3 shows the match between observed and synthetic waveforms for the minimum misfit solution returned by the inversion routine. The inversion in Fig. 3 was performed with a water layer of 2 km depth on top of an 8 km thick layer of $V_P = 4.5\ \mathrm{km\ s^{-1}}$ (representing the sediment cover), which was above a half-space of $V_P = 6.8\ \mathrm{km\ s^{-1}}$. The prominent pulses at about 17 s after the *P* arrival and about 25 s after the *SH* arrival are reflected phases from the sea surface and sea bed, and provide the main constraint on centroid depth, given the velocity structure.

In Fig. 3 the estimated centroid depth is 41 km. It is probable that this event occurred in the mantle, and thus we may reasonably expect a significant reflection coefficient from the Moho as well as from the sediment–basement interface, though neither is likely to be as large as those from the top and bottom of the water layer. Ideally, our velocity structure would include both sediment and basement layers above a mantle half-space: but the inversion routine of McCaffrey & Abers (1988) is restricted to a single layer (plus a water layer) above a half-space. We therefore experimented with a variety of layer and half-space combinations to see what effect thay had on the match of observed and synthetic seismograms and on the estimated values of seismic moment and centroid depth (Fig. 4).

The first row of Fig. 4 contains 3 *P* and 4 *SH* seismograms from Fig. 3. Rows 2 and 3 show seismograms at the same stations having altered the velocity structure and allowed the inversion routine to change only the centroid depth, seismic moment and amplitudes of the time function elements. For the second row we change the thickness of the sediment layer from 8 to 18 km (covering the range estimated by Makris & Stobbe 1984). The match of seismograms is perhaps slightly worse than in the first row, and the centroid depth is shallower, because of the slower average velocity above the source. For the third row we replaced the

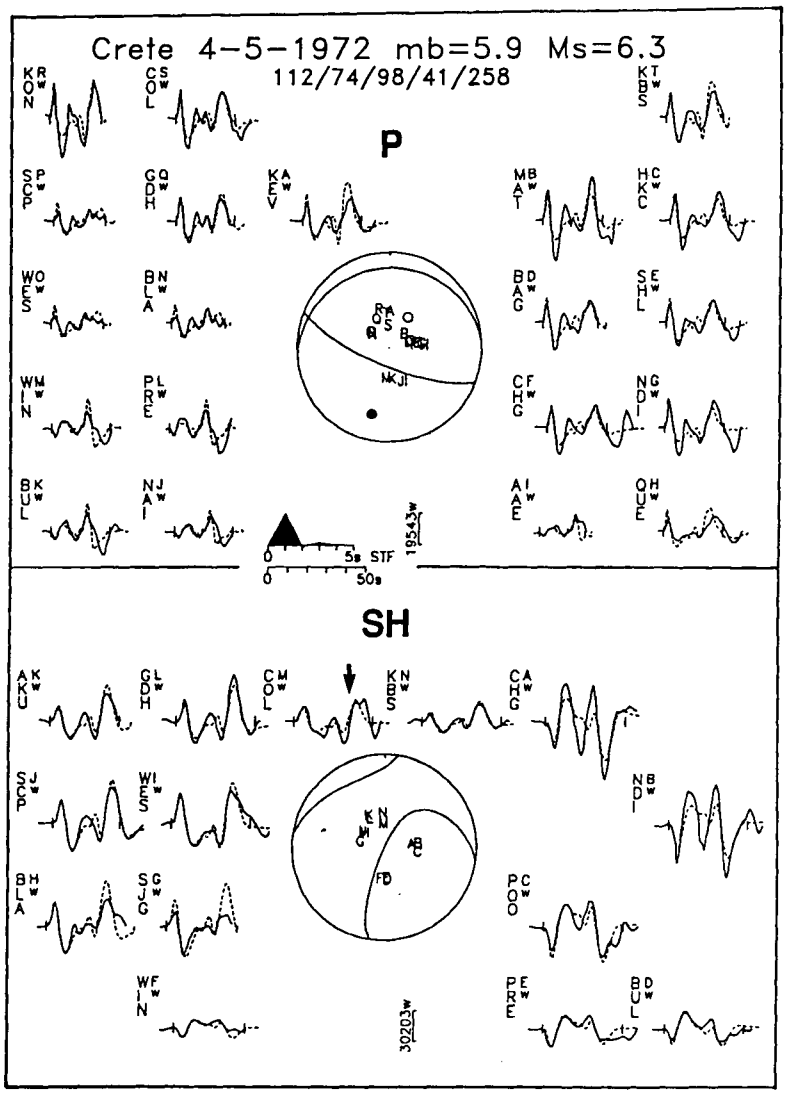

Figure 3. This (and subsequent similar figures) shows the radiation patterns and synthetic waveforms for the minimum misfit solution returned by the inversion routine, as well as the observed waveforms. For the purposes of display, waveform amplitudes have been normalized to that of an instrument with a gain of 3000 at a distance of 40°. Solid lines are observed waveforms, and the inversion window is identified by vertical bars. Synethetic waveforms are dashed lines. The station code is identified to the left of each waveform, together with an upper case letter, which identifies its position on the focal sphere, and a lower case letter that identifies the type of instrument (w = WWSSN long period; s = WWSSN short period; d = GDSN long period). The vertical bar beneath the focal spheres shows the scale in microns, with the lower case letter identifying the instrument type, as before. The source time function is shown in the middle of the figure, and beneath it is the time-scale used for the waveforms. Focal spheres are shown with *P* and *SH* nodal planes, in lower hemisphere projection. Station positions are indicated by letter, and are arranged alphabetically clockwise, starting from north. *P* and *T* axes are marked by solid and open circles. Where *ScS* is expected to arrive within the inversion window its predicted arrival time is marked with a black arrow (e.g. for COL in this figure). Beneath the header at the top of the figure, which shows the date, body wave and surface wave magnitudes, are five numbers which show the strike, dip, rake, centroid depth and seismic moment (in units of 10^{16} N m) of the minimum misfit solution.

sediment layer with a crust 25 km thick, a likely value immediately south of Crete, and with $V_P = 6.0\,\mathrm{km\,s^{-1}}$, similar to the average crustal velocity found by Makris *et al.* (1983), above a mantle half-space of $V_P = 7.6\,\mathrm{km\,s^{-1}}$. This will have altered the take-off angles of rays leaving the source (by less than 5° in the teleseismic distance range). The match between observed and synthetic seismograms is, if anything, better in the third row than in the first, and, though the centroid depth has changed by only 2 km, the seismic moment has increased by 40 per cent. In row 3 the improved match of seismograms between the direct arrival and the reflections from the water layer is caused by reflection from the interface, mimicking the Moho, 12 km above the source. This can be seen also in row 4, in which the top layer consists of 18 km of sediments ($V_P = 4.5\,\mathrm{km\,s^{-1}}$) above a mantle of $V_P = 7.6\,\mathrm{km\,s^{-1}}$. In this case the inversion routine returned a depth of 34 km, because of the slower average velocity above the source, thus placing the source 14 km below the velocity discontinuity. The inversion in row 4 was performed with all source parameters, except the duration of the time function, free to change, illustrating what little effect the velocity structure

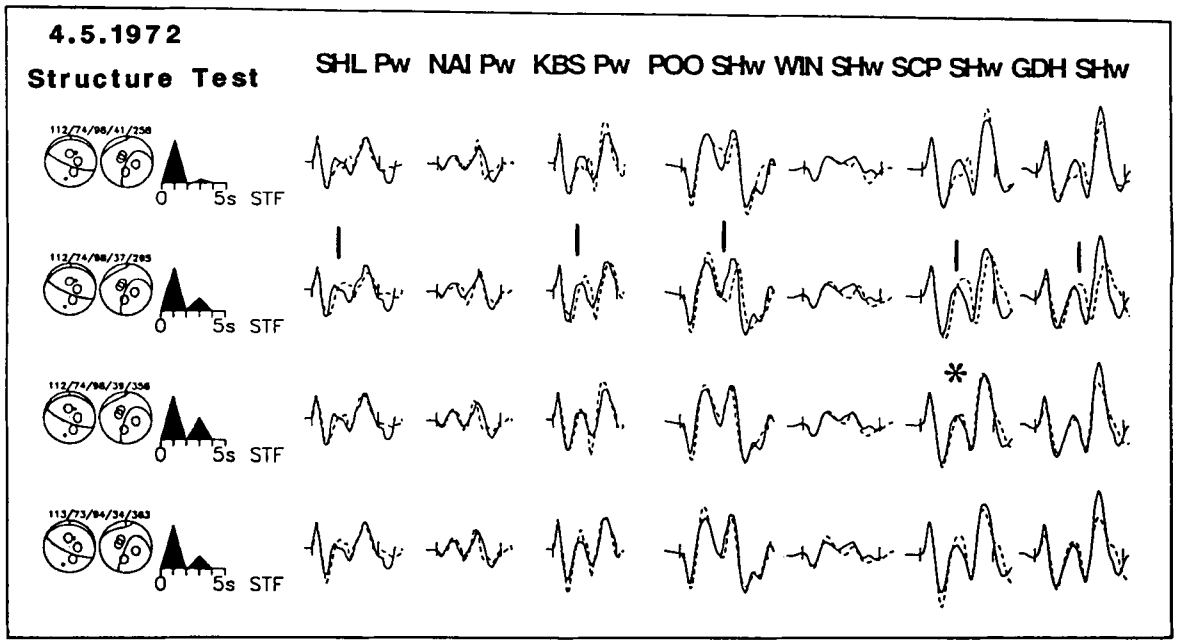

Figure 4. In this (and subsequent similar figures) each row shows a selection of waveforms from a run of the inversion program. The top row always shows waveforms from the minimum misfit solution. The stations are identified at the top of each column, with the type of waveform marked by *P* or *SH* and followed by the instrument type, as in Fig. 3. At the start of each row are the *P* and *SH* focal spheres for the focal parameters represented by the five numbers above (strike, dip, rake, depth, moment, as in (Fig. 3), showing the positions on the focal spheres of the stations chosen. To the right is the source time function. The displayed waveforms are in the same convention as Fig. 3, but in this type of figure the large bars show matches of observed to synthetic waveforms that are worse than in the minimum misfit solution, and asterisks show matches that are improvements (see also Molnar & Lyon-Caen 1989). Fig. 4 investigates the effect of source velocity structure on the source time function, centroid depth and moment returned by the inversion routine (see text). The velocity structure used for each row is as follows:

	Layer	V_P (km s^{-1})	V_S (km s^{-1})	density (kg m^{-3})	thickness (km)
row 1:	1	1.5	0.0	1030	2
	2	4.5	2.6	2420	8
	3	6.8	3.9	2910	half-space
row 2:	1	1.5	0.0	1030	2
	2	4.5	2.6	2420	18
	3	6.8	3.9	2910	half-space
row 3:	1	1.5	0.0	1030	2
	2	6.0	3.5	2820	25
	3	7.6	4.4	3300	half-space
row 4:	1	1.5	0.0	1030	2
	2	4.5	2.6	2420	18
	3	7.6	4.4	3300	half-space

exercised on the estimates of strike, dip and rake. Although the match of seismograms in row 4 is good, the velocity structure used is clearly unrealistic.

We conclude from these experiments that the velocity structure in the source region, which is uncertain, may lead to a shift in centroid depth estimates of up to about 4 km, and an uncertainty in moment of at least 40 per cent. The computational restriction to one layer (plus water) above a half-space is not serious, given the uncertainty in the real structure anyway. More complex velocity models may be enticing because of their apparent realism, but we have no confidence that their centroid depth estimates are likely to be superior. For the earthquakes of 1972 May 4, and others in the depth range around 35–42 km, we used the velocity model of row 1 in Fig. 4 (see Table 1) for subsequent inversions and tests. This has the disadvantage that the source is embedded in material of $V_P = 6.8$ km s^{-1} rather than in the mantle, where it almost certainly occurred, but the advantage that the upper sedimentary layer has the same velocity (and thickness) as for the shallower events (Table 1); the similarity in reflection coefficients at the base of the water layer will thus tend to bias moment estimates in the same way for all events. The velocity structue used in row 1 is, if anything, likely to be too slow for events at 40 km depth, and the depths obtained for these events are thus likely to be rather too shallow (by up to 4 km based on Fig. 4): but they will all be biased the same way.

It is tempting to infer from the improved match of

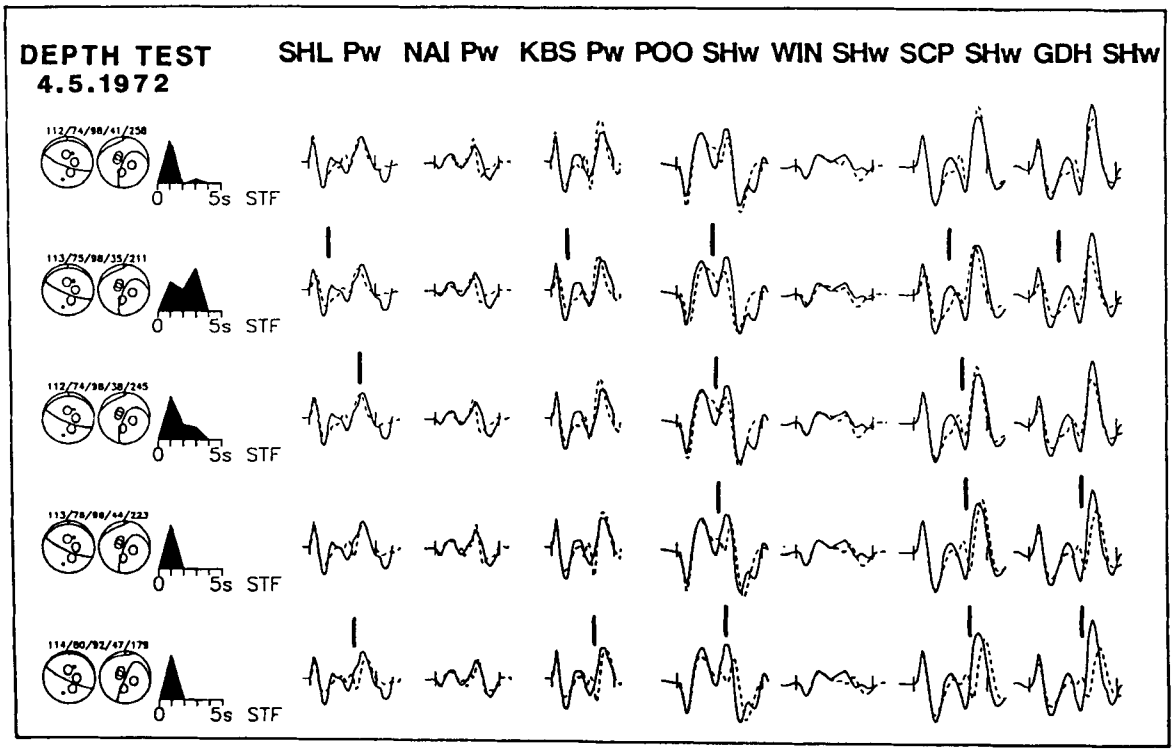

Figure 5. This figure follows the convention of Fig. 4. The top row is the minimum misfit solution. In rows 2–5 the depth has been held fixed at 35, 38, 44 and 47 km, while the other parameters were left free.

seismograms between the direct and surface reflections in rows 3 and 4 of Fig. 4 that the centroid of the event is around 12–14 km below the Moho. This is indeed consistent with our estimate of centroid depth (around 40 km) and with Makris & Stobbe's (1984) estimate of Moho depth in the vicinity (25–30 km), but we are not confident that it is well resolved.

Next, in Fig. 5, we examine how well centroid depth is resolved, having chosen a velocity structure (that of row 1 in Fig. 4). Row 1 again displays the minimum misfit solution, and rows 2 to 5 display waveforms from inversions in which all source parameters were free to change except the centroid depth, which was fixed to values of 35, 38, 44 and 47 km. The observed fit between observed and synthetic waveforms is clearly worse in rows 2–4 than in row 1. For this group of events with centroid depths in the region of 40 km, there is a clear separation between direct phases and surface reflections, and centroid depth was well resolved, with the waveforms poorly matched if the depth was fixed to 3 to 5 km either side of the value found in the free inversion. Note that the values of strike, dip and rake are little different in rows 2–5 from those in row 1.

In Fig. 6 we demonstrate a similar test for strike. In this group of events that involved thrusting on E–W planes we solve for the steep nodal plane dipping south, because that is probably the auxiliary plane, and its strike determines the azimuth of the slip vector, which is a parameter we wish to determine. The format of Fig. 6, and of subsequent similar figures, follows that of Fig. 5. Row 1 displays the minimum misfit solution, and in lower rows are the results of inversions in which one parameter (in this case the strike) is held fixed and the others are free to change. The match of waveforms is noticeably worse in rows 2–4 than that in row 1, even for a strike value 12° or 13° different from that of the free solution. Note particularly the degradation of *SH* waveform at the southern station WIN: the waveform at this station is sensitive to strike as it is close to a nodal plane for *SH*. The uncertainty in strike (and hence slip vector) for this event is less than 10°. Note, however, that waveforms at some stations show a slight improvement when a parameter (in this case strike) is set at a value that is clearly unacceptable because of the poor fit at other stations (e.g. KBS and SCP in row 4): an effect that was remarked on by Molnar & Lyon-Caen (1989).

Dip is examined in Fig. 7. The dip of the steep nodal plane is constrained by the polarities of the first motions at southern stations (Fig. 2), and cannot be more than about 5° smaller than its minimum misfit value, though it could be larger by up to 10°.

Rake (Fig. 8) is the least well-determined parameter, and can vary up to 20° from the minimum misfit solution before the match of waveforms seriously deteriorates. The rake determines the dip and strike of the gently dipping nodal plane. The allowable uncertainty in rake means that we cannot determine whether that plane dips gently NW or NE: though its dip must be small ($< 20°$).

Thus, based on the experiments in Figs 5–8, the parameters and uncertainties we estimate for this event are: strike $112 \pm 10°$ (though this is further restricted by first motion polarities); dip 74 $-5/+10°$; rake $98 \pm 20°$, and depth 41 ± 2 km (though this does not allow for uncertainty related to the velocity structure). Our results are similar to those of Kiratzi & Langston (1989): strike 130°; dip 72°; rake 90°, and depth 40 km (we also obtain the same moment and source duration). The main difference between our results is in the strike, and probably arises from their

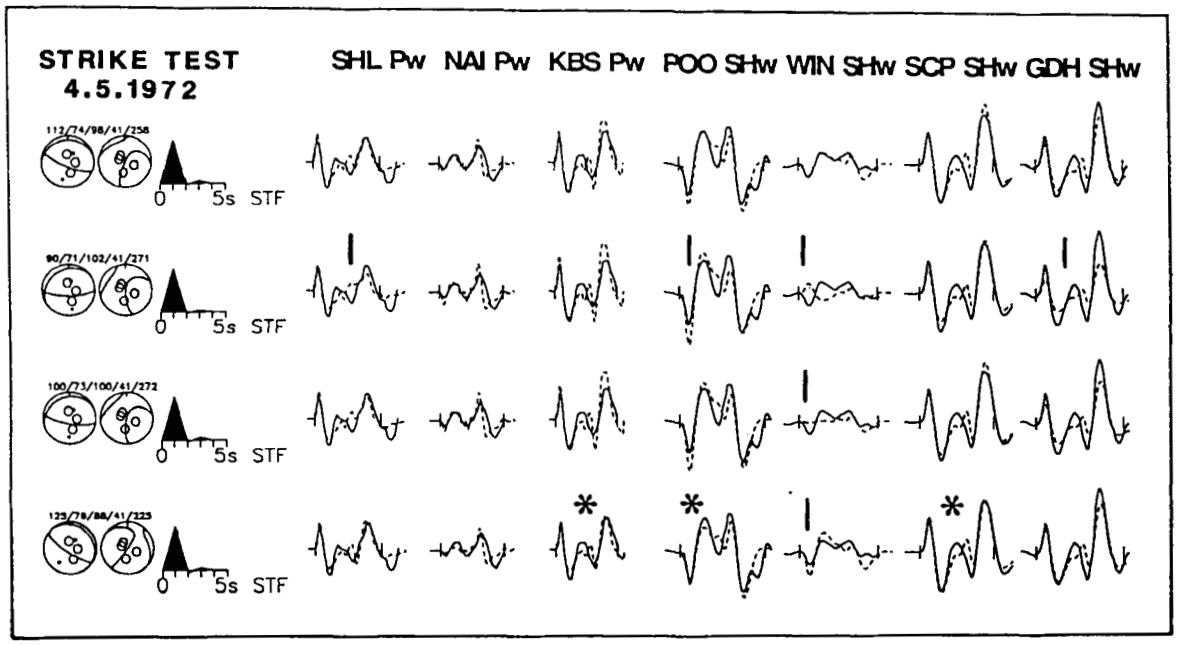

Figure 6. In this figure the top row is the minimum misfit solution. In rows 2–4 the strike has been held fixed at 90°, 100° and 125°, while the other parameters have been left free. The display convention is that of Fig. 4.

inversion not being restricted to a double couple mechanism: Kiratzi & Langston (1989) inverted for five independent elements of the moment tensor (the requirement for no volume change removing the sixth from the inversion), and obtained a non-double couple component, represented by a compensated linear vector dipole, of 17.4 per cent. This might, as they suggest, be a measure of source complexity. Alternatively, it might be expected from any attempt to match the observed seismograms with synthetic waveforms generated in a velocity structure that does not vary with azimuth, as in reality it surely does in this source region. For this reason, we prefer an inversion in

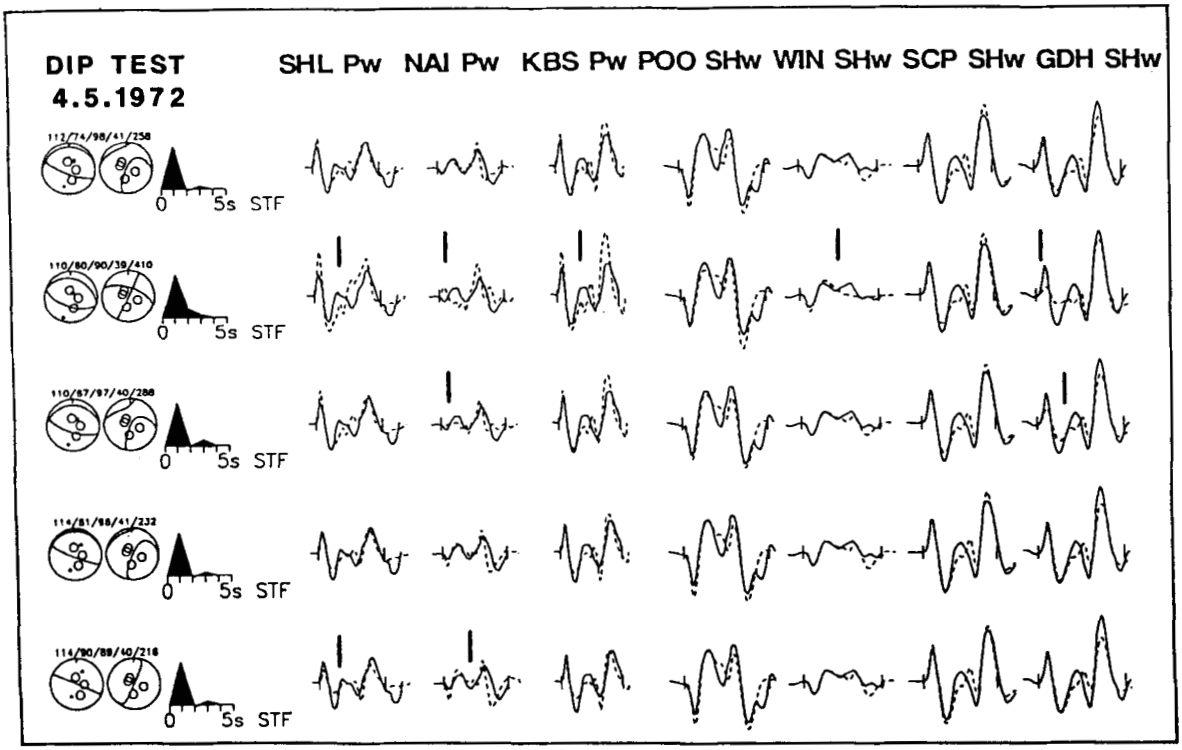

Figure 7. In rows 2–5 of this figure the dip has been held fixed at values of 60°, 67°, 81° and 90°, while the other parameters have been left free. The display convention is that of Fig. 4.

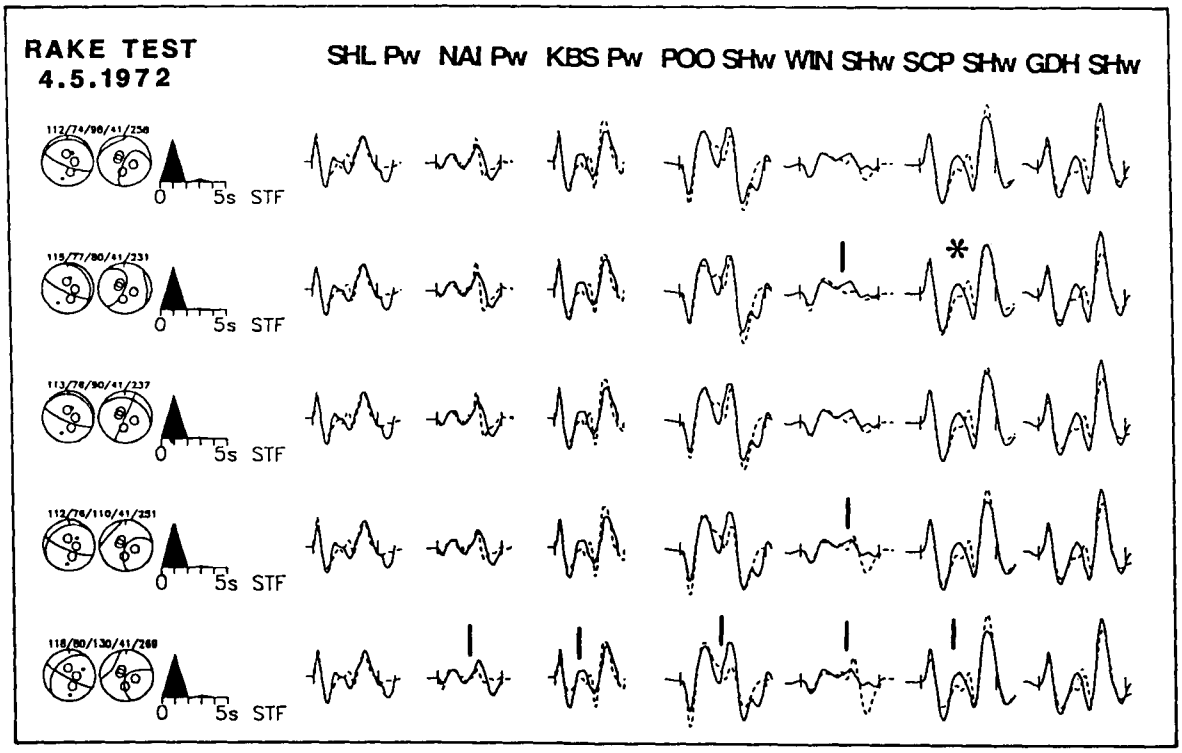

Figure 8. In rows 2–5 of this figure the rake has been fixed at values of 80°, 90°, 110° and 130°, while the other parameters have been left free. The display convention is that of Fig. 4.

which the source is constrained to be a double couple: we then investigate source complexity explicitly, by inverting for the time function, and, if necessary, also for later sources (or subevents) with a different orientation and depth. The uncertainties given by Kiratzi & Langston (1989) are for the individual moment tensor elements of the non-double couple source, and are not easily translated into the uncertainties in strike, dip and rake of the major double couple.

The earthquake of 1969 June 12

This event had a centroid depth in the region of 20 km, much shallower than that of 1972 May 4, and almost certainly above the Moho. Its mechanism was also different, involving thrust faulting on roughly N–S planes, with an E–W *P* axis. There were three other events in our study with similar centroid depths and mechanisms. For all of them we used a source velocity structure consisting of a layer of water above an 8 km thick layer of sediments with $V_P = 4.5\ \mathrm{km\,s^{-1}}$, which overlay a half-space of $V_P = 6.5\ \mathrm{km\,s^{-1}}$. The minimum misfit solution is hown in Fig. 9, and has a source orientation that is consistent with first motion polarities, shown in Fig. 2.

The resolution of centroid depth is examined in Fig. 10, in which the format is the same as Fig. 5. A fixed depth 4 km shallower than the minimum misfit depth produces a marginally worse fit for *SH*-waveforms at HKC and BEC (row 2). A fixed depth 6 km deeper (row 3) produces a misfit that is more obvious. We estimate that the uncertainty in centroid depth for this event is about ±5 km. To demonstrate that the event must be shallower than that of 1972 May 4, we performed inversions at fixed depths of 30 and 35 km (rows 4 and 5): the misfit is clearly unacceptable. Note that the source orientation in rows 2–5 is little different from that in the minimum misfit solution (row 1).

Strike is examined in Fig. 11. The *SH*-waveforms at COL and WIN are nodal, and very sensitive to a reduction in strike of even 10°. On the other hand, an increase in strike of up to 25° can be tolerated without seriously affecting the waveforms. Note that there is some trade-off between strike and dip if strike is fixed to 20° or more greater than the minimum misfit value.

Dip is examined in Fig. 12. The dip can be increased only 5° before seriously affecting the waveforms, but may be reduced by up to about 20°. Here too, the trade-off between strike and dip is apparent, while the values of rake and depth are stable.

The ability to resolve rake is shown in Fig. 13. If the rake is fixed more than 15° either side of the minimum misfit value the match of waveforms deteriorates, though once again, the inversion routine tries to compensate by changing the dip and strike.

Our estimated parameters and uncertainties for this earthquake are therefore: strike 163 −10/+25°; dip 50 +5/−20°; rake 44 ± 15°, and depth 19 ± 5 km.

Other earthquakes

Other earthquakes are discussed in the Appendix. For all of them except that of 1979 June 15, whose solution is not well determined, we carried out tests similar to those described in Figs 4–8 and 10–13 to estimate uncertainties in strike, dip, rake and centroid depth. Their source parameters, and

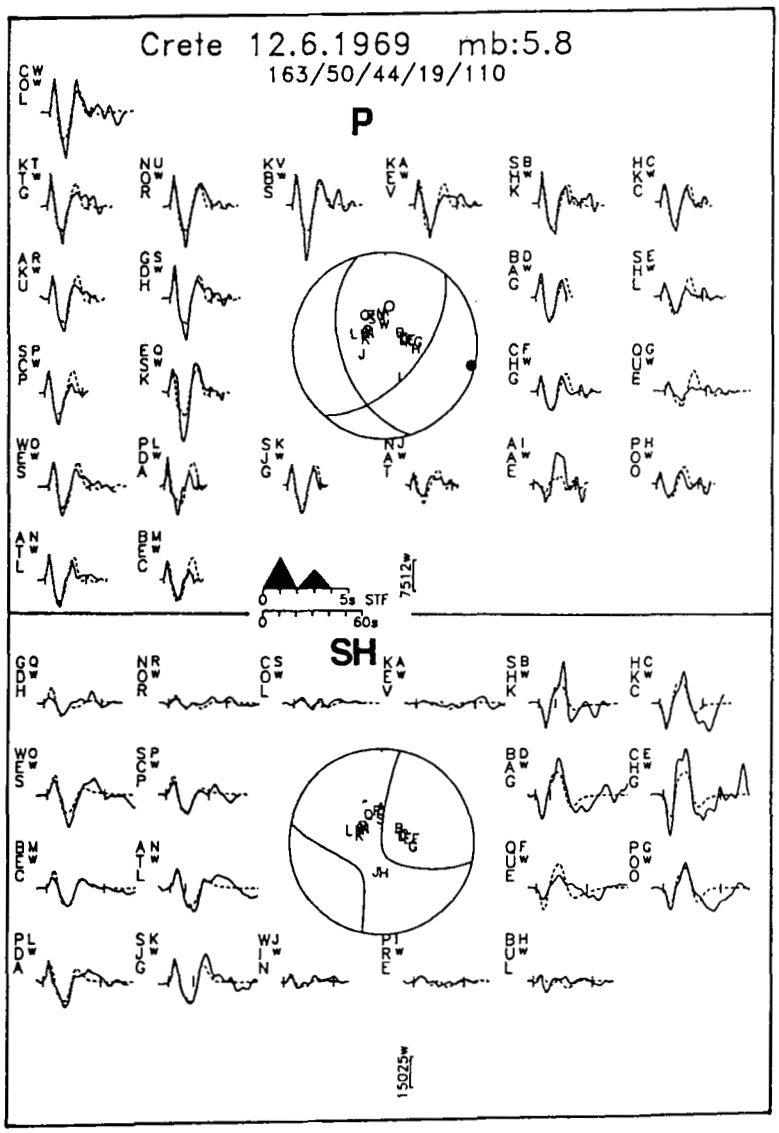

Figure 9. The minimum misfit solution for the earthquake of 1969 June 12. The display convention is that of Fig. 3. The short *SH* windows for some distant stations were chosen to avoid prominent *ScS* arrivals.

our estimates of their uncertainties, are summarized in Table 2. Their ISC locations are listed in Table 1.

3 EARTHQUAKE LOCATIONS

The earthquakes we studied are located in Fig. 14 at their epicentres determined by the ISC (International Seismological Centre). These locations are likely to be affected by the heterogeneous mantle structure expected in the vicinity of the subduction zone, and may be considerably in error. There is little we can do to correct the absolute locations of any of these events, as no dense seismograph network exists on Crete that could constrain them. We can, however, investigate the relative locations of these earthquakes, using differential arrival time data. We did this using the technique described by Jackson & Fitch (1979). Like all relative location techniques, this one assumes that velocity anomalies along the ray paths occur outside the immediate source region encompassing master and secondary events, and so should not be used for events separated by a greater distance than that over which this assumption is reasonable. We therefore used two master events: that of 1984 June 21 (M1 in Fig. 15) and that of 1983 March 19 (M2 in Fig. 15). The locations of the other earthquakes relative to these two master events are shown in Fig. 15, and tabulated in Table 3. Most of the relocations use more than 150 stations and have standard errors in relative epicentre of less than 3 km. Relative depths were unconstrained in the relocation and are not expected to be accurate: nonetheless, the relative depths found by this technique are not absurd (Table 3), which is probably an indication that the relative epicentres are reasonably well resolved. The relative pattern of epicentres we obtained is not significantly different from the relative pattern of epicentres found by the ISC (Fig. 15). Note that those events relocated relative to both masters have almost the same locations in both cases, so that the relative separation between the two masters is probably close to that given by the ISC. Of course, the whole pattern

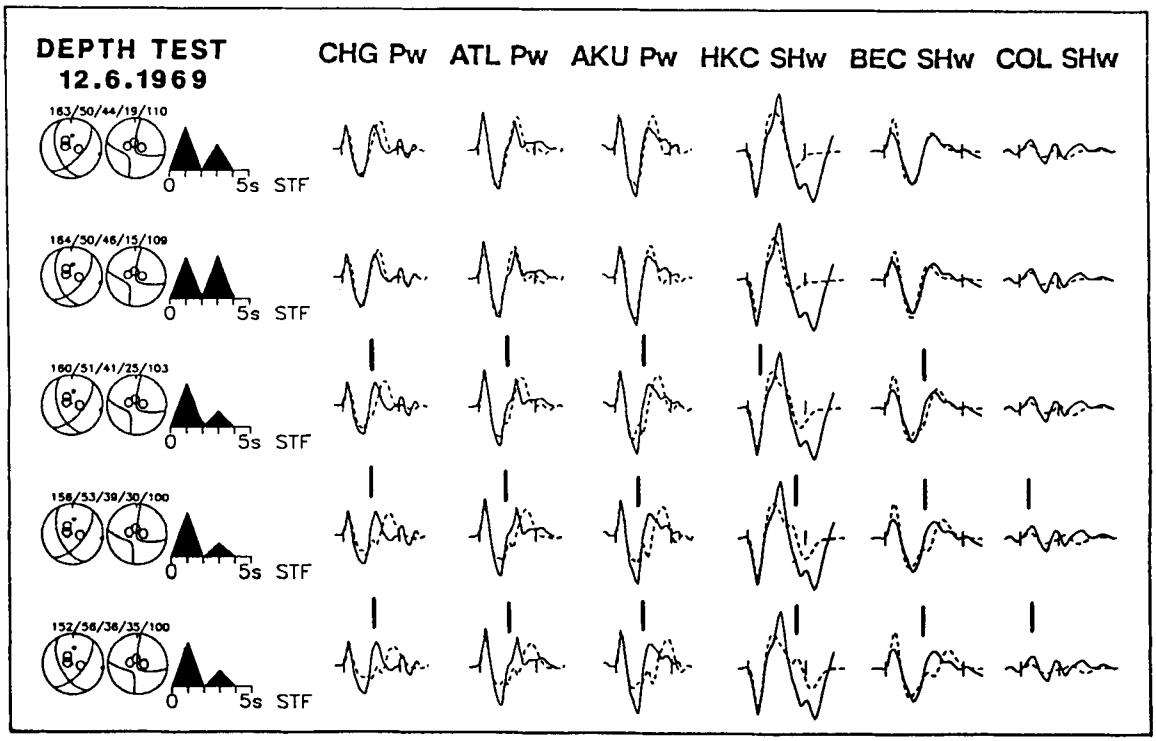

Figure 10. In rows 2–5 of this figure the depth has been held fixed at 15, 25, 30, and 35 km, while the other parameters were free to vary. The top row is the minimum misfit solution. The display convention is that of Fig. 4.

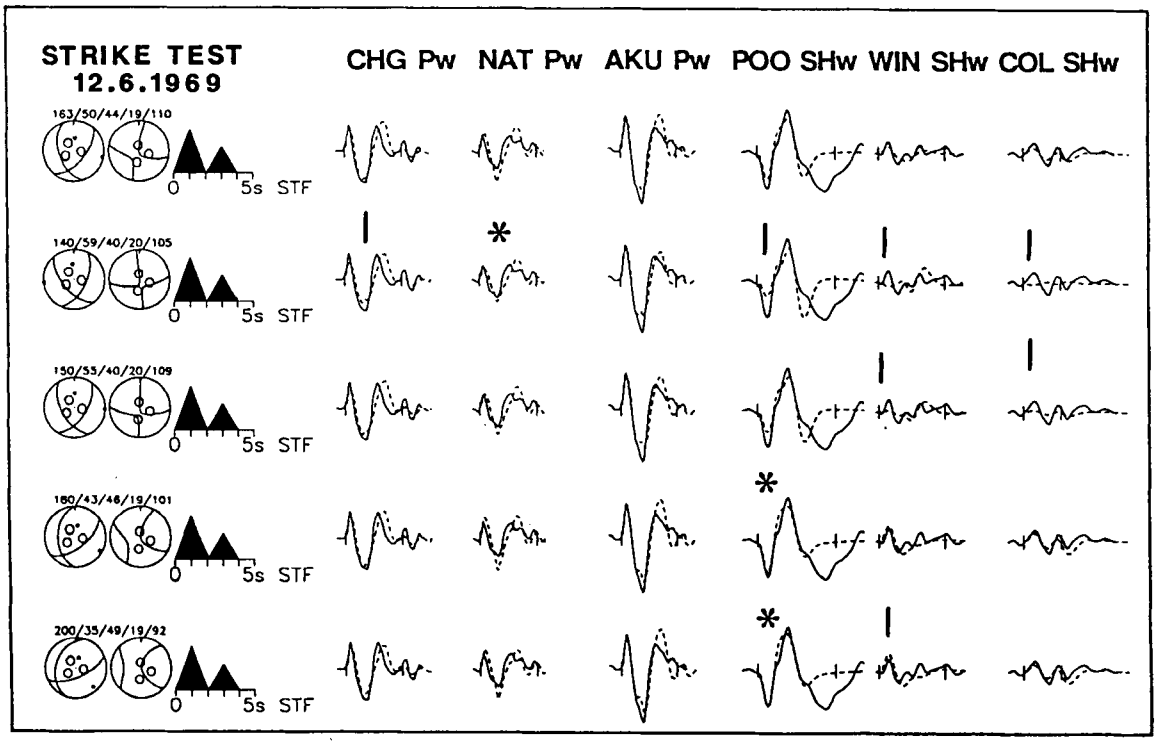

Figure 11. In rows 2–5 of this figure the strike has been fixed at values of 140°, 150°, 180° and 200°, while the other parameters have been left free. The display convention is that of Fig. 4.

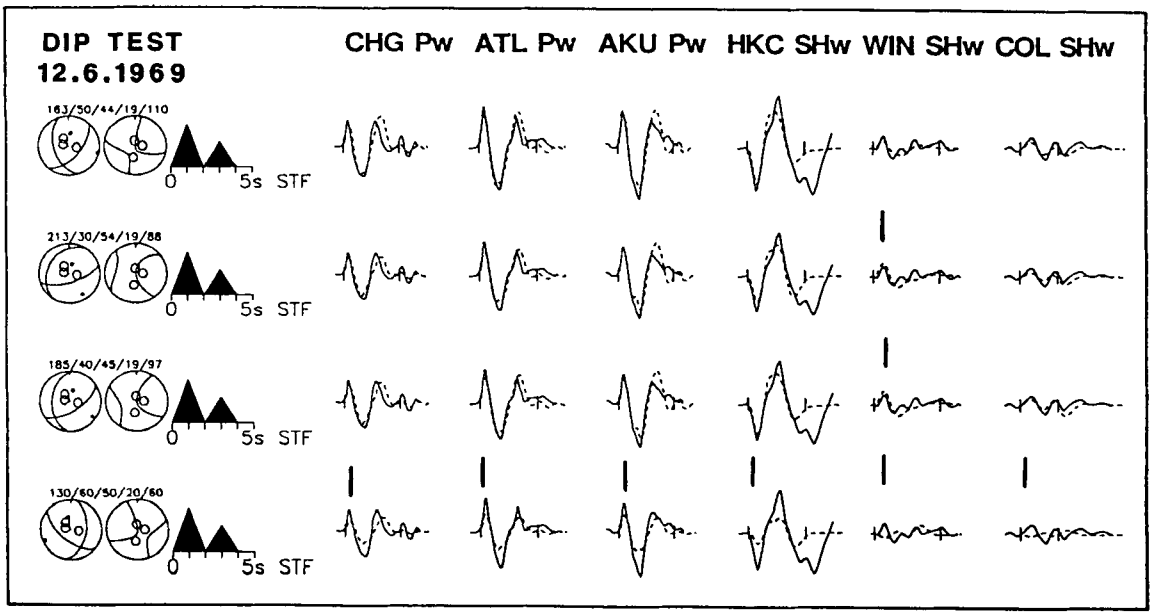

Figure 12. In rows 2–4 of this figure the dip has been fixed at values of 30°, 40° and 60°, while the other parameters have been left free. The display convention is that of Fig. 4.

could be shifted in absolute coordinates. We have illustrated it using the ISC locations for the two masters which, because each was located with more than 450 stations, are unlikely to be wrong by more than about 20 km. For the purposes of later discussion, note that the event of 1982 August 17 is confirmed to be almost 200 km south of western Crete, probably beneath the Mediterranean Ridge, and that the two events of 1966 May 9 and 1985 September 27 are confirmed to be SE of the rest of the group, probably beneath the deep basin SE of Crete (Fig. 1).

4 INTERPRETATION OF FOCAL MECHANISMS

The focal mechanisms and centroid depths for the earthquakes in this study are shown in Fig. 14. The mechanisms fall into four groups: (a) normal faulting; (b) low-angle thrusting on approximately E–W planes; (c) high-angle reverse faulting on approximately E–W planes; and (d) high-angle reverse faulting with some strike-slip motion, on planes with a NW to NE strike, and with

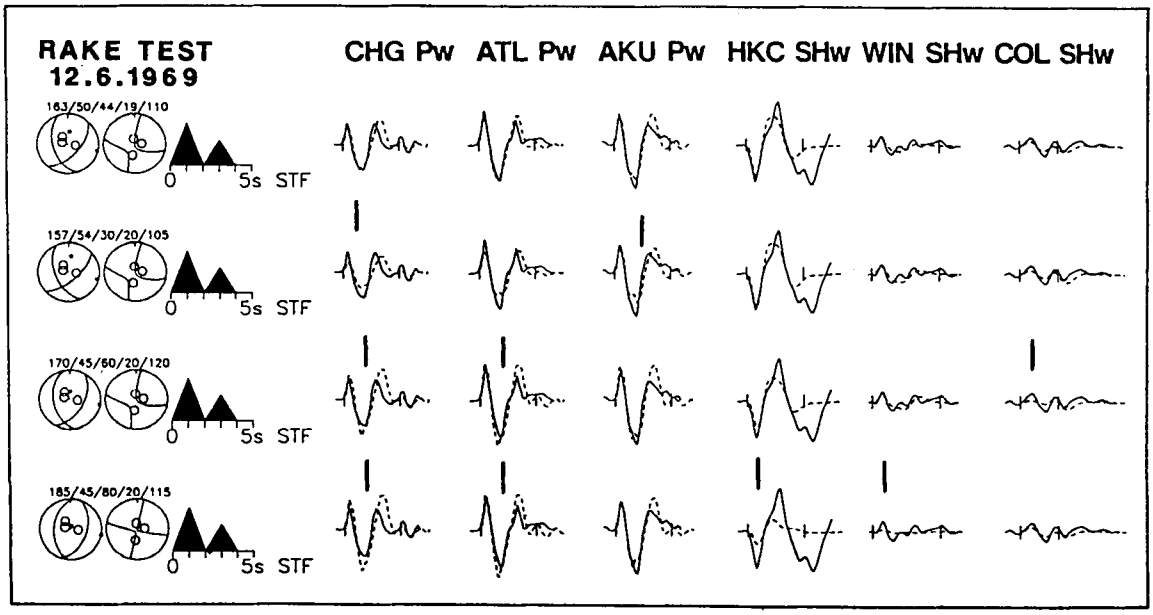

Figure 13. In rows 2–4 of this figure the rake has been fixed at values of 30°, 60° and 80°, while the other parameters have been left free. The display convention is that of Fig. 4.

Table 2. Earthquake source parameters and estimated uncertainties.

									ERRORS					
#	Date	Str.	Dip	Rake	h	Mo	Ms	mb	Str.	Dip	Rake	h	P	SH
1	9.Apr.1965	63	76	157	51	151	--	6.0	± 7	± 5	± 4	± 6	10	13
3	9.May.1966	132	46	110	16	22	--	5.5	±15	±10	±15	-4/+2	13	6
4	12.Jun.1969	163	50	44	19	110	--	5.8	-10/+25	-20/+5	±15	± 5	23	19
5	4.May.1972	112	74	98	41	258	6.3	5.9	±10	-5/+10	±20	± 2	20	14
6	29.Nov.1973*	224	67	10	18	54	--	5.7	±15	±10	±10	± 4	12	6
		236	45	77	19	30								
7	22.Sep.1975	209	75	131	64	29	--	5.4	±12	±15	±10	± 4	8	7
8	18.Aug.1977	114	79	96	38	20	--	5.5	±15	±10	±20	± 4	12	3
9	11.Sep.1977*	276	47	89	19	84	--	5.8	±10	± 4	±10	-5/+3	21	9
		248	77	5	19	50								
10	15.May.1979	253	17	65	35	39	5.4	5.5	±13	-7/+5	±10	± 4	10	11
11	15.Jun.1979	150	75	70	40	35	4.9	5.5	--	--	--	--	4**	2
12	17.Aug.1982	230	45	109	39	300	6.6	6.0	-20/+15	±10	±20	± 7	22	9
13	19.Mar.1983	44	51	139	67	30	5.0	5.7	±10	± 5	-10/+20	± 6	6	5
14	21.Jun.1984	110	72	83	39	120	5.9	5.8	± 8	-4/+10	± 7	± 5	21	18
15	27.Sep.1985	125	77	9	38	55	5.2	5.6	±10	±10	-5/+10	± 4	4	6

* Multiple event with different solutions seems to be required.
** P waveforms used are Short-Period vertical component records.
Mo in units of 10^{16} Nm.

approximately E–W *P* axes. Two earthquakes, on 1973 November 29 and 1985 September 27, do not obviously fall into these categories.

We have only one normal faulting event (group a). This was the earthquake of 1965 April 27 (no. 2 in Fig. 14b), studied by McKenzie (1972) and Lyon–Caen *et al.* (1988). In Fig. 14 the mechanism and depth for this event are those of Lyon–Caen *et al.* (1988), and are constrained by *P*- and *SH*-waveforms. The mechanism shows normal faulting on N–S planes, which is seen along the entire southern edge of the Aegean as it over-rides the subducting African plate: in the Peloponnese, in western Crete (responsible for the prominent peninsulas in the NW corner of Crete), and in the offshore regions in between (McKenzie 1978; Angelier *et al.* 1982; Lyon–Caen *et al.* 1988). Ekstrom & England (1989) give a moment-tensor solution for a small (m_b 5.2) event on 1979 July 23 NE of Crete (35.5°N, 26.3°E) with a similar mechanism and depth to that of 1965 April 27. This faulting represents extension parallel to the arc within the material above the subduction zone.

The four earthquakes with low-angle thrust faulting mechanisms on E–W planes (group b) have centroid depths in the range 35–41 km. The two high-angle reverse fault mechanisms with similar strikes (group c) have shallower centroid depths. The slip vectors in both groups are similar: all of them being between N and NNE (Fig. 16). If they all involve thrusting on north-dipping planes, then a reasonable interpretation of their mechanisms is that the low-angle thrusts occur on a large structure separating the subducting African plate from the over-riding block, and that the high-angle reverse faults represent splay faulting off this master thrust surface: as illustrated in the cross-section in Fig. 17.

The fourth group (d) have centroid depths that are, on the whole, deeper than the others. Four of them (numbers 1,7,12 and 13 in Fig. 14b) clearly occur within the subducting African lithosphere. These all show *P* axes trending roughly E–W and *T* axes trending roughly N–S (Fig. 17d), with a suggestion that the events in the west have *P* axes WNW–ESE, whereas those in the east have *P* axes more closely E–W (Fig. 18). Five of the more northerly events have *T* axes aligned approximately with the dip direction of the sinking African lithosphere (Fig. 17d), as in other subduction zones that do not extend to great depths (Isacks & Molnar 1971). The earthquake of 1979 June 15 (no. 11 in Fig. 14b) has a centroid depth close to that of the low-angle thrusts: however its mechanism in Fig. 14 is very different from them and clearly places it in group (d). The mechanism of this event is the least well constrained in our study, with no long-period *P*-waveforms that were large enough to digitize and only two *SH*-waveforms. Nonetheless, a combination of first motion polarities and *SH*-waveforms is sufficient to demonstrate that the mechanism is more likely to be similar to that of group (d) than those of groups (b) or (c) (see Appendix).

Two events are distinctive because they involve largely strike–slip motion. The earthquake of 1973 November 29 (no. 6 in Fig. 14b) has a centroid depth (18 km) that places it clearly in the material over-riding the subduction zone. We do not know which nodal plane is the fault plane, but if it is the plane striking NE–SW then the slip vector is almost the same as that of the low- and high-angle thrusts. The event of 1985 September 27 (no. 15 in Fig. 14b) has a *P* axis trending E–W, suggesting a similarity with events within the subducting lithosphere, but, if the NE–SW nodal plane is the fault plane, it could have a slip vector the same as those of the low- and high-angle thrusts (Fig. 16). Its centroid depth (38 km) is close to the postulated depth of the master thrust fault of the subduction zone, and it could belong to either group. However, because the epicentre of this event is close to the Pliny and Strabo branches of the Hellenic Trench, which are thought to be sites of left-lateral faulting on NE–SW planes (e.g. McKenzie 1978; Le Pichon & Angelier 1979), the right-lateral motion in this event suggests

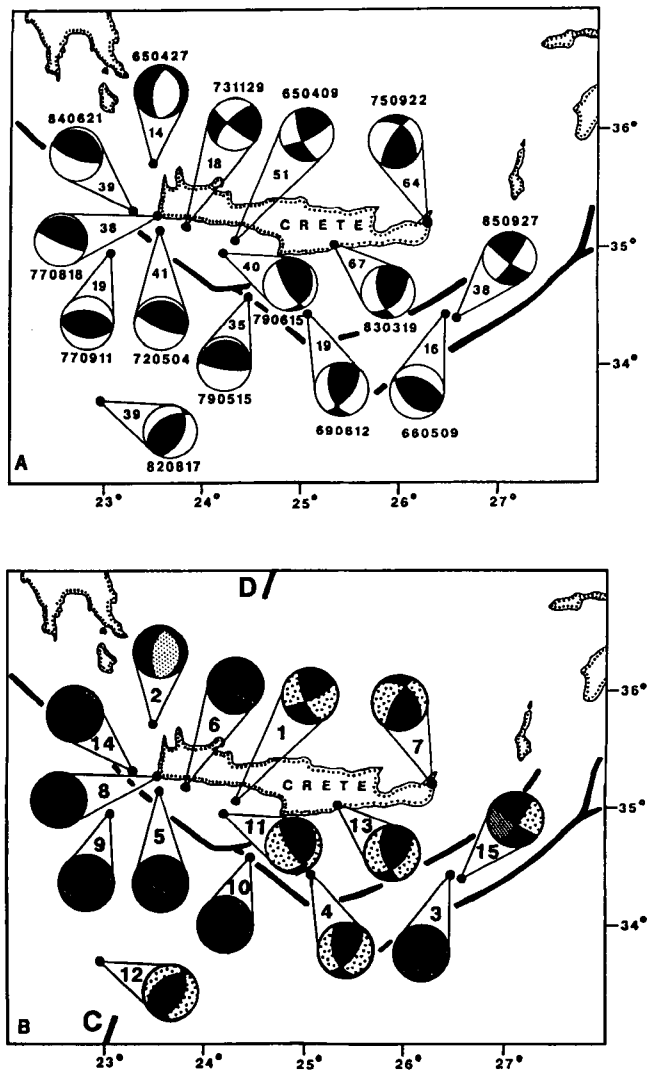

Figure 14. (a) This figure shows the minimum misfit fault plane solutions of the earthquakes studies in this paper. That of 1965 April 27 is from Lyon-Caen *et al.* (1988). Focal spheres are lower hemisphere equal area projections, with compressional quadrants shaded. Next to each sphere is the date of the event (year, month, day) and enclosed in the two lines joining the sphere to its ISC epicentre is the centroid depth in km. The dark lines show the deepest parts of the various branches of the Hellenic Trench, adapted from Angelier *et al.* (1982). (b) The same fault plane solutions as in (a), but with shading of the dilatational quadrants to show to which group each belongs in our analysis. The normal fault NW of Crete (group a) has dense stippling. Thrust or reverse faulting on roughly E–W planes and the shallow strike–slip fault in SW Crete (groups b and c) have dark shading. These earthquakes all have one slip vector with a NNE orientation. The events with roughly E–W *P* axes and N–S *T* axes (group d) are lightly stippled. Note that the earthquake of 1985 September 27 (no. 15) has the shading of both groups (b)/(c) and (d), as it could belong to either, though our preference is for group (d) (see text). The numbers next to each sphere identify each event in the cross-section along the line C–D (Fig. 17) and in Tables 1 and 3.

an affinity with group (d), rather than with groups (b) and (c).

The focal mechanisms and centroid depths thus reveal a reasonably clear pattern. The convergence between the African lithosphere and the Aegean is represented by the

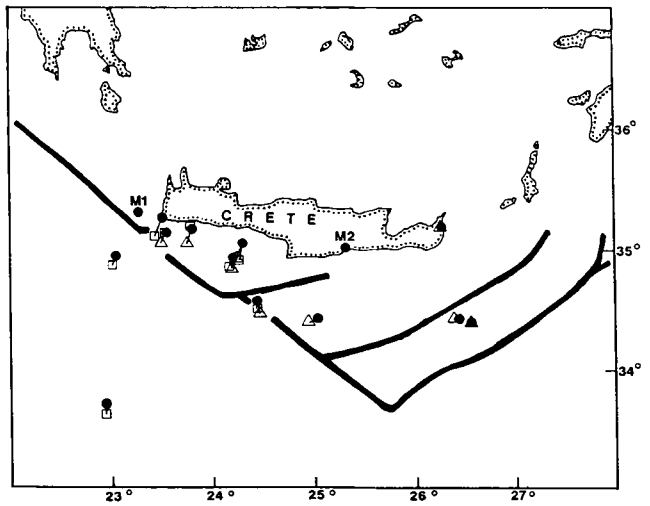

Figure 15. Filled circles are ISC epicentres of the events in this study. Open squares are relocations relative to master event M1 west of Crete. Open triangles are relocations relative to master event M2 in central Crete. Both master events have been kept in their ISC locations. Details of the relocations are given in Table 3. The dark lines indicate the axes of the Hellenic Trench system.

low- and high-angle thrust faulting, with an average slip vector of 021° ± 10°, or 025° ± 12° if the two strike slip events are included. Farther north, normal faulting with a N–S strike occurs at shallow depths, indicating E–W extension within the over-riding wedge. Earthquakes within the subducting African lithosphere have *T* axes aligned N–S, presumably inidicating the expected pull of the subducting slab, but also ESE–WNW *P* axes, suggesting shortening roughly parallel to the arc. The only obvious exception to this pattern is the earthquake of 1969 June 12 (no. 4 in Fig. 14b), which clearly belongs to the group with ESE–WNW *P* axes, yet has a relatively shallow (19 km) centroid depth. The bathymetry in its epicentral region (Fig. 1) shows that it was associated with an anomalously shallow part of the seafloor south of Crete. The nature of this shallow region is unknown: it may be an area of thicker basement (and thinner sediment cover) within the subducting African crust, and active thrusting with an E–W strike may outcrop at the base of the steep escarpment farther north close to the coast of Crete. It is clear from both the bathymetry and vertical movements of the coastline (Flemming 1978) that the structure of the seafloor in the trench changes mid way along the length of Crete, and perhaps we are not justified in projecting all the earthquakes on to a single cross-section, as in Fig. 17.

5 DISCUSSION

The pattern of earthquake focal mechanisms and depths discussed above has several implications for the tectonics of the Hellenic arc system near Crete.

The system of high-angle imbricate reverse faults, which is likely to merge with low-angle thrust faulting at depth, is presumably responsible for thickening and scraping the sediment off the subducting African plate. Limited isotopic data suggests that little of this sediment is incorporated into the Aegean arc volcanic rocks (Barton *et al.* 1983; Briqueu

Table 3. Results of relative relocations.

	DATE	AZI	POL	LENGTH	LAT	LON	DEPTH	h	ELAT	ELON	EDEP	STA	RMS
14;	21. 6.1984	(MASTER)			35.31N	23.28E	39.0					450	
1;	9. 4.1965	115.76	91.55	100.38	34.92	24.27	36.3	51	2.15	0.10	1.73	178	1.13
5;	4. 5.1972	126.87	95.03	30.05	35.14	23.54	36.4	41	1.55	0.41	1.65	146	1.12
6;	29.11.1973	104.16	81.51	48.93	35.20	23.79	46.2	18	1.59	0.67	1.51	146	1.25
8;	18. 8.1977	145.68	86.23	25.99	35.11	23.44	40.7	38	1.37	0.55	1.46	178	1.04
9;	11. 9.1977	206.48	113.42	58.84	34.87	23.01	15.6	19	0.15	0.93	1.44	199	1.03
10;	15. 5.1979	129.68	83.74	139.45	34.51	24.45	54.2	35	1.54	0.11	1.56	205	1.21
11;	15. 6.1979	121.32	90.21	95.50	34.86	24.17	38.6	40	1.51	0.05	1.62	170	1.10
12;	17. 8.1982	189.41	95.74	190.40	33.62	22.93	19.9	39	0.54	0.89	1.38	287	1.18
13;	19. 3.1983	(MASTER)			35.02N	25.32E	67.0					400	
1;	9. 4.1965	264.26	107.62	103.02	34.93	24.24	35.8	51	2.11	1.07	4.12	83	0.98
3;	9. 5.1966	124.07	107.16	122.80	34.42	26.38	30.7	16	1.66	0.58	2.96	92	1.18
4;	12. 6.1969	206.19	114.79	84.22	34.40	24.95	31.7	19	0.38	1.35	2.71	123	0.97
5;	4. 5.1972	271.49	100.12	167.94	35.05	23.50	37.5	41	2.03	0.65	2.99	128	1.08
6;	29.11.1973	271.66	100.16	144.36	35.05	23.76	41.5	18	1.84	0.79	3.02	146	1.27
7;	22. 9.1975	77.45	86.31	87.48	35.19	26.25	72.6	64	1.20	1.60	2.48	154	0.93
10;	15. 5.1979	231.60	103.14	100.86	34.47	24.47	44.1	35	0.30	1.63	2.42	208	0.99
11;	15. 6.1979	259.00	106.07	108.14	34.84	24.20	37.1	40	1.43	0.94	2.72	170	0.87
15;	27. 9.1985	125.53	103.35	142.38	34.29	26.55	34.1	38	1.57	0.13	2.26	236	0.73

AZI,POL and LENGTH define the vector joining the master event to the secondary.
AZI is the azimuthal angle measured from North, POL is the take-off angle measured from the downwards vertical, and LENGTH is in kilometres.
h is the centroid depth obtained from waveform modelling.
ELAT,ELON and EDEP are the standard errors of the latitude, longitude and depth of the location, in kilometres.
STA is the number of stations used in the relocation.
RMS is in seconds.

et al. 1986), presumably because it is not transported deep enough into the mantle for melting to occur. Instead the sediment probably underplates Crete and is responsible for its general uplift, as suggested by Angelier *et al.* (1982). In western Crete, where there is the cluster of low- and high-angle thrust events in Fig. 14, notches and marine terraces in limestone indicate rapid uplift in the Holocene (Flemming 1978). Uplifted coastlines are seen along the western half of the southern coast of Crete, with an abrupt change to lesser uplift, or subsidence, about midway along the southern coast. The bathymetry (Fig. 1) also shows a change at about longitude 24.5°: to the west is the shallow but submerged Gavdos Rise, and to the east is a less well-defined shallow region. The two rises are separated by a deep re-entrant valley along a steep escarpment adjacent to the southern coast of central Crete. We suspect, from the bathymetry and seismicity, that the steep submarine escarpments south of both the Gavdos Rise and the rise farther east are bathymetric expressions of steep north-dipping imbricate reverse faults that reach the surface (Fig. 17b). Le Pichon *et al.* (1982a) report sea-beam observations demonstrating that extensional faulting is seen at the sea surface as far south as the inner wall of the Hellenic Trench. This extensional faulting is presumably underlain by active shortening on thrust faults, suggesting that it may represent near-surface collapse structures, possibly cutting no deeper than the Miocene evaporites know to outcrop in the inner trench wall (Le Pichon *et al.* 1982a). Our observations are compatible with Le Pichon *et al.*'s (1982a) suggestion that shortening occurs within the subducting lithosphere and sedimentary pile, but not significantly within the over-riding Aegean material east of the SW-facing boundary of the Hellenic Trench and north of the Pliny trough. There is no evidence of normal faulting earthquakes south of the coast of Crete. Le Pichon *et al.* (1982a) also report shortening in the outer wall of the Hellenic Trench south of Crete on

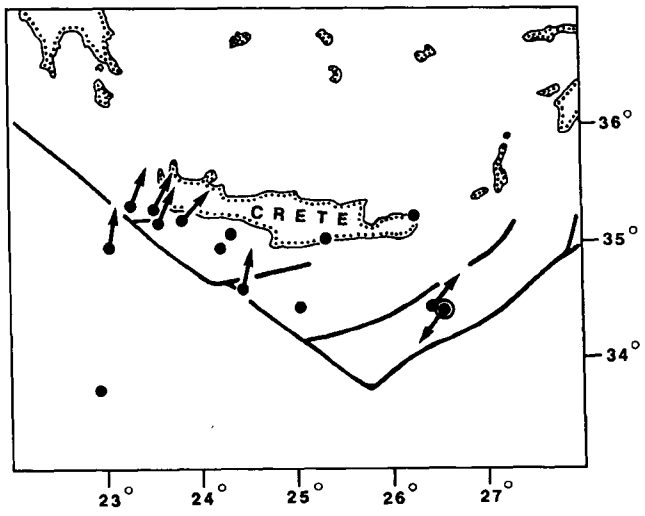

Figure 16. Horizontal projections of slip vectors for the earthquakes in groups (b) and (c) are shown by arrows. The sense of slip shown is that of the south side relative to the north side. The reasons for chosing one of the two possible slip vectors are discussed in the text. The slip vector for the event of 1985 September 27, which we suspect belongs to group (d), is identified by a circle. The dark lines indicate the axes of the Hellenic Trench system.

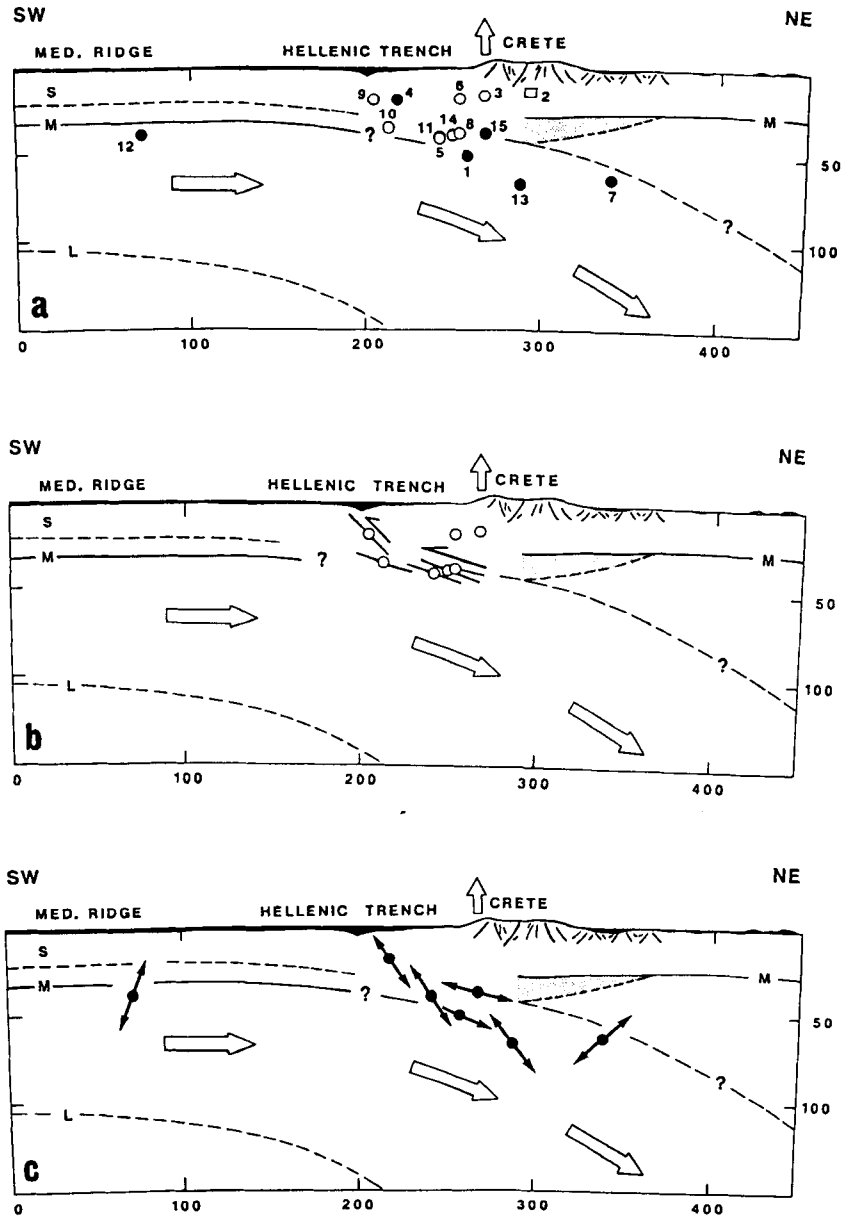

Figure 17. Cross-sections along the line C–D in Fig. 14. Sea water is shown in black. Sediment (S) thickness south of Crete, and Moho depth (M) are estimated from the work of Makris (1977), Makris *et al.* (1983) and Makris & Stobbe (1984). Sediments (light stippling) are shown underplating Crete, after Angelier *et al.* (1982). **(a)** Hypocentres are shown using the centroid depths from the minimum misfit solutions, with numbers identifying the events in Fig. 14 and Tables 1 and 3. The square is the normal faulting event off NW Crete. Open circles are events of group (b) and (c) (those with a NNE slip vector). Filled circles are events of group (d) (those with E–W *P* axes). **(b)** Events of groups (b) and (c) are shown with the projection of the nodal plane dipping N for the thrust and reverse faults, with arrows indicating the sense of slip. **(c)** Events of group (d) are shown with arrows indicating the dip of their *T* axes. **(d)** Lower hemisphere projection of the *P* (filled circles) and *T* (filled squares) axes of the events in group (d). The axes for the event of 1985 September 27 are enclosed by circles: this event may have an affinity with groups (b) and (c) as it has one slip vector with a SSW projection (Fig. 16). The approximate dip and strike of the subducting slab are also shown.

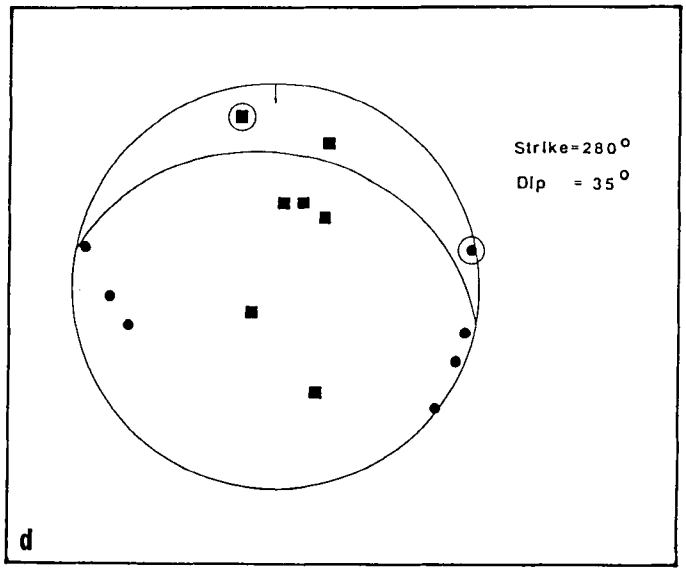

Figure 17. (*continued*)

thrust faults that dip to the south. Whether these continue into basement or are restricted to the sedimentary cover is unclear: there is little seismicity beneath the outer wall of the trench (Fig. 1), and there have been no events large enough for us to investigate.

The thickening of sediments above the subducting African plate continues at least 100–150 km south of Crete, and is probably responsible for the shallow bathymetry and deformation of the Mediterranean Ridge, as suggested by numerous people (e.g. Ryan *et al.* 1970; Ryan, Kastens & Cita 1982; Kenyon, Belderson & Stride 1982; Le Pichon *et al.* 1982b). The deformation of the Mediterranean Ridge is complex and greatly affected by diapiric and dissolution structures (Ryan *et al.* 1982; Le Pichon *et al.* 1982b), but the presence of the earthquake of 1982 August 17 (no. 12 in Fig. 14b) shows that it is not strictly thin-skinned. This earthquake was certainly in basement and probably in the uppermost mantle. Its mechanism has more in common with the other earthquakes within the subducting plate farther north, which have *P* axes trending WNW–ESE. It does not have the mechanism expected if the basement were to take

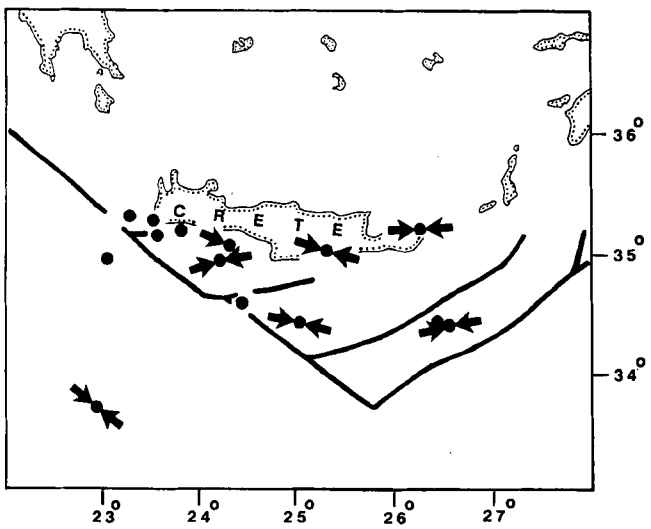

Figure 18. Projections of the *P* axes of events in group (d).

up N–S shortening beneath decoupled sediments that are largely folded. Le Pichon *et al.* (1982b) report that the fold axes in the epicentral region of this earthquake trend roughly E–W, and hypothesize that the NNE direction of shortening seen within the uppermost layers of the Mediterranean Ridge reflects the deeper strain pattern. The mechanism of the 1982 August 17 earthquake, which shows WNW–ESE shortening, casts doubt on this conclusion. The earthquake of 1982 August 17 occurred near the highest elevation of the Mediterranean Ridge, where its crescent shape appears to have been indented by the Libyan margin (Le Pichon *et al.* 1982b). Makris & Stobbe (1984) suggest that the Mediterranean Ridge is the submerged leading edge of the stretched African continental margin, now inverted by shortening. It may be similar in this respect to the Zagros mountains in SW Iran (Jackson 1980) but, unlike the Zagros, there is no evidence in the basement beneath the Mediterranean Ridge for high-angle reverse faulting earthquakes with a strike parallel to that of the overlying folds.

If we are right to separate the earthquake mechanisms into the groups discussed above, the slip vectors of the low-angle thrusts and other events at shallower depths may be used to estimate the convergence direction between the Mediterranean Sea floor and Crete. To do this we have to assume that the north-dipping nodal planes are the fault planes, which seems reasonable on geological grounds and is consistent with the bathymetry. The average direction we obtain is 021° ± 10° excluding the two strike–slip events, and 025° ± 12° if they are included and their NE-striking nodal planes are taken to be the fault planes. These values compare with the 045° estimated by Le Pichon & Angelier (1979), who used first motion solutions by McKenzie (1972, 1978) and Ritsema (1974), and McKenzie's (1978) own estimate of 031°. Our focal mechanisms are better constrained than those on which these earlier estimates were based, and our slip vectors show less scatter: so we expect our estimate to be an improvement on that of McKenzie (1978) and Le Pichon & Angelier (1979). There is another reason for the improvement. It is clear from the discussion above that several of the earthquakes in this region do not have mechanisms and depths that should be interpreted as directly reflecting the convergence between the Mediterranean Sea and Crete: instead they indicate deformation within the subducting plate. In the absence of well-constrained depths and mechanisms, the pattern described here was not apparent to Le Pichon & Angelier (1979) who, quite reasonably, used all the events, and obtained a correspondingly large scatter of slip vectors. Note, however, that the convergence direction of around 020° may only apply to the SW-facing boundary of the Hellenic Trench (i.e. west of 25°E). On the SE-facing boundary there are only two mechanisms (numbers 3 and 15 in Fig. 14b) with slip vectors of 42° and 035°, one of which (no. 15) may belong to group (d) anyway.

The reservations expressed above also apply to the work by Jackson & McKenzie (1988a, b) and Tselentis *et al.* (1988), who used all the events in the Hellenic Trench to estimate the seismic contribution to the rate of convergence. Although it is clear from their work that the seismicity can only account for a maximum of 10 per cent of the convergence, the observation presented here suggest that even this is an overestimate, as several of the earthquakes

they included are likely to represent deformation within the subducting plate.

The deformation within the subducting plate requires some explanation. There is no evidence for normal faulting seaward of the trench with a strike parallel to arc, as in other subduction zones. The N–S trending *T* axes, with several of them aligned approximately down the dip of the subducting slab, presumably represent the pull of the subducted lithosphere, as seen elsewhere in slabs that do not penetrate to 400 km (Isacks & Molnar 1971). The *P* axes that trend roughly E–W, almost parallel to the strike of the arc in this region, are less obviously explained. One possibility is that the eastern Mediterranean Sea floor is in a state of E–W compression from a cause unrelated to the subduction: suggestions include the high topography that surrounds the basin, or even ridge push from the Mid-Atlantic. Such explanations are not easily tested.

ACKNOWLEDGMENTS

This research would not have been done without the help of R. McCaffrey, whose program and guidance were essential. We thank the station operators of WWSSN stations, and the staff at the data centre at the British Geological Survey, Edinburgh. We are grateful to Helene Lyon-Caen for providing some of the seismograms. We would like to thank Dan McKenzie, Keith Priestley and Helene Lyon-Caen for many helpful discussions and improvements to an early version of this paper. We thank X. Le Pichon for a perceptive and helpful review. T.T. is grateful for encouragement and support from N. White, C. Peirce, J. Collier, and A. Smith. This work was supported by the Turkish Ministry of Higher Education and NERC. Cambridge Earth Sciences contribution no. 1729.

REFERENCES

Angelier, J., Lyberis, N., Le Pichon, X., Barrier, E. & Huchon, P., 1982. The tectonic development of the Hellenic arc and the Sea of Crete: a synthesis, *Tectonophysics*, **86,** 159–196.

Barton, M., Salters, V. & Huijsmans, J., 1983. Sr-isotope and trace element evidence for the role of continental crust in calc-alkaline volcanism on Santorini and Milos, Aegean Sea, Greece, *Earth planet. Sci. Lett.*, **63,** 273–291.

Briqueu, L., Javoy, M., Lancelot, J. R. & Tatsumoto M., 1986. Isotope geochemistry of recent magmatism in the Aegean arc: Sr, Nd, Hf, and O isotopic ratios in the lavas of Milos and Santorini-geodynamic implications, *Earth planet. Sci. Lett.*, **80,** 41–54.

Chase, C. G., 1978. Plate kinematics: the Americas, East Africa, and the rest of the world, *Earth Planet. Sci. Lett.*, **37,** 355–368.

Comninakis, P. E. & Papazachos, B. C., 1980. Space and time distribution of the intermediate focal depth earthquakes in the Hellenic arc, *Tectonophysics*, **70,** T35–T47.

Dercourt, J. *et al.*, 1986. Geological evolution of the Tethys belt from the Atlantic to the Pamirs since the Lias, *Tectonophysics*, **123,** 241–315.

Dziewonski, A. M., Friedman, A. & Woodhouse, J. H., 1983a. Centroid-moment tensor solutions for January–March, 1983, *Phys. Earth planet. Inter.*, **33,** 71–75.

Dziewonski, A. M., Friedman, A., Giardini, D. & Woodhouse, J. H., 1983b. Global seismicity of 1982: centroid-moment tensor solutions for 308 earthquakes, *Phys. Earth planet. Inter.*, **33,** 76–90.

Dziewonski, A. M., Franzen, J. E & Woodhouse, J. H., 1985. Centroid-moment tensor solutions for April–June, 1984, *Phys. Earth. planet. Inter.*, **37,** 87–96.

Dziewonski, A. M., Franzen, J. E & Woodhouse, J. H., 1986. Centroid-moment tensor solutions for July–September 1985, *Phys. Earth planet. Inter.*, **42,** 205–214.

Ekstrom, G. & England, P. C., 1989. Seismic strain rates in regions of distributed continental deformation, *J. geophys Res.*, **94,** 10 231–10 257.

Flemming, N. C., 1978. Holocene eustatic changes and coastal tectonics in the northeast Mediterranean: implications for models of crustal consumption, *Phil. Trans. R. Soc. Lond.*, **289,** 405–458.

Fredrich, J., McCaffrey, R. & Denham, D., 1988. Source parameters of seven large Australian earthquakes determined by body waveform inversion, *Geophys. J.*, **95,** 1–13.

Futterman, W. I., 1962. Dispersive body waves, *J. geophys. Res.*, **67,** 5279–5291.

Huchon, P., Lyberis, N., Angelier, J., Le Pichon, X. & Renard, V., 1982. Tectonics of the Hellenic Trench: A synthesis of sea-beam and submersible observations, *Tectonophysics*, **86,** 69–112.

IOC–UNESCO, 1981. *International Bathymetric Chart of the Mediterranean*, scale 1:1 000 000, 10 sheets, Ministry of Defence, Leningrad.

Isacks, B. & Molnar, P., 1971. Distribution of stresses in the descending lithosphere from a global survey of focal mechanism solutions of mantle earthquakes, *Rev. Geophys.*, **9,** 103–174.

Jackson, J. A., 1980. Reactivation of basement faults and crustal shortening in orogenic belts, *Nature*, **283,** 343–346.

Jackson, J. A. & Fitch, T. J., 1979. Seismotectonic implications of relocated aftershock sequences in Iran and Turkey, *Geophys. J. R. astr. Soc.*, **57,** 209–229.

Jackson, J. A. & McKenzie, D., 1984. Active tectonics of the Alpine–Himalayan Belt between western Turkey and Pakistan *Geophys. J. R. astr. Soc.*, **77,** 185–264.

Jackson, J. A. & McKenzie, D., 1988a. The relationship between plate motions and seismic moment tensors, and the rates of active deformation in the Mediterranean and the Middle East, *Geophys. J.*, **93,** 45–73.

Jackson, J. A. & McKenzie, D., 1988b. Rates of active deformation in the Aegean Sea and surrounding area, *Basin Res.*, **1,** 121–128.

Kenyon, N. H., Belderson, R. H. & Stride, A. H., 1982. Detailed tectonic trends on the central part of the Hellenic Outer Ridge and in the Hellenic Trench System, in *Trench-Forearc Geology: Sedimentation and Tectonics in Modern and Ancient Active Plate Margins,* Spec. Publ. Geol. Soc. Lond., vol. 10, pp. 335–343, ed. Leggett, J. K., Blackwell Scientific Publications, Oxford.

Kiratzi, A. A. & Langston, C. A., 1989. Estimation of earthquake source parameters of the May 4, 1972 event of the Hellenic arc by the inversion of waveform data. *Phys. Earth planet. Inter.*, **57,** 225–232.

Kissel, C. & Laj, C., 1988. The Tertiary geodynamical evolution of the Aegean arc: a paleomagnetic reconstruction, *Tectonophysics,* **146,** 183–201.

Le Pichon, X. & Angelier, J., 1979. The Hellenic arc and trench system: a key to the evolution of the eastern Mediterranean area, *Tectonophysics*, **60,** 1–42.

Le Pichon, X. *et al.* 1982a. Subduction in the Hellenic Trench: probable role of a thick evaporitic layer based on Seabeam and submersible studies, in *Trench-Forearc Geology: Sedimentation and Tectonics in Modern and Ancient Plate Margins,* Spec. Publ. Geol. Soc. Lond., Vol. 10, pp. 319–333, ed. Leggett, J. K., Blackwell Scientific Publications Oxford.

Le Pichon, X., Lyberis, N., Angelier, J. & Renard, V., 1982b. Strain distribution over the East Mediterranean Ridge: A synthesis incorporating new Sea-Beam data, *Tectonophysics*, **86,** 243–274.

Lyon-Caen, H. *et al.*, 1988. The 1986 Kalamata (South

Peloponnesus) Earthquake: Detailed study of a normal fault, evidence for east–west extension in the Hellenic Arc, *J. geophys. Res.*, **93,** 14 967–15 000.

Main, I. G. & Burton, P. W., 1989. Seismotectonics and the earthquake frequency-magnitude distribution in the Aegean area, *Geophys. J. R. astr. Soc.*, **98,** 575–586.

Makris, J., 1977. Geophysical investigations of the Hellenides, *Hamburger Geophysikalische Einzelschriften*, vol. 34, University of Hamburg.

Makris, J. & Stobbe, C., 1984. Physical properties and state of the crust and upper mantle of the Eastern Mediterranean sea deduced from geophysical data, *Mar. Geol.*, **55,** 347–363.

Makris, J., Ben Abraham, Z., Behle, A., Ginzburg, A., Giese, P., Steinmetz, L., Whitmarsh, R. B. & Eleftheriou, S., 1983. Seismic refraction profiles between Cyprus and Israel and their interpretation, *Geophys. J. R. astr. Soc.*, **75,** 575–591.

Martin, C., 1988. Geometrie et Cinematique de La Subduction Egéenne: structure en vitesse et en attenuation sous Le Pelopponnese, *Thesis*, University of Grenoble.

McCaffrey, R., 1988. Active tectonics of the Eastern Sunda and Banda Arcs, *J. geophys. Res.*, **93,** 15 163–15 182.

McCaffrey, R. & Nabelek, J., 1987. Earthquakes, gravity, and the origin of the Bali Basin: an example of a nascent continental fold-and-thrust belt, *J. geophys. Res.*, **92,** 441–460.

McCaffrey, R. & Abers, G., 1988. SYN3: A program for inversion of teleseismic body wave forms on microcomputers, *Air Force Geophysics Laboratory Technical Report*, AFGL-TR-88-0099, Hanscomb Air Force Base, MA.

McKenzie, D., 1972. Active tectonics of the Mediterranean Region, *Geophys. J. R. astr. Soc.*, **30,** 109–185.

McKenzie, D., 1978. Active tectonics of the Alpine–Himalayan belt: the Aegean Sea and surrounding regions, *Geophys. J. R. astr. Soc.*, **55,** 217–254.

Mercier, J. L., Sorel, D., Vergely, P. & Simeakis, K., 1989. Extensional tectonic regimes in the Aegean basins during the Cenozoic, *Basin Res.*, **2,** 49–71.

Meulenkamp, J. E., Wortel, M. J. R., Van Wamel, W. A., Spakman, W. & Hoogerduyn Strating, E., 1988. On the Hellenic subduction zone and the geodynamic evolution of Crete since the late Middle Miocene, *Tectonophysics*, **146,** 203–215.

Molnar, P. & Lyon-Caen, H., 1989. Fault plane solutions of earthquakes and active tectonics of the Tibetan Plateau and its margins, *Geophys. J. Int.*, **99,** 123–153.

Nabelek, J. L., 1984. Determination of earthquakes source parameters from inversion of body waves, *PhD thesis*, MIT, MA.

Nelson, M. R., McCaffrey, R. & Molnar, P., 1987. Source parameters for 11 earthquakes in the Tien Shan, Central Asia, determined by P and SH waveform inversion, *J. geophys. Res.*, **92,** 12 629–12 648.

Papazachos, B. C., 1973. Distribution of seismic foci in the Mediterranean and surrounding area and its tectonic implications, *Geophys. J. R. astr. Soc.*, **33,** 419–428.

Ritsema, A. R., 1974. The earthquake mechanisms of the Balkan region, *R. Netherl. Meteorol. Inst., De Bilt, Sci Rep.*, 74–4.

Ryan, W. B. F., Kastens, K. A. & Cita, M. B., 1982. Geological evidence concerning compressional tectonics in the Eastern Mediterranean, *Tectonophysics*, **86,** 213–242.

Ryan, W. B. F., Stanley, D. J., Hersey, J. B., Fahlquist, D. A. & Allan, T. D., 1970. The tectonics and geology of the Mediterranean Sea, in *The Sea*, vol. 4, II, pp. 387–492, Wiley Interscience, New York.

Sellers, P. C. & Cross, P. A., 1989. 1986 and 1987 Wegener–Medlas baselines determined using the Pseudo-Short Arc Technique, in *Proceedings Int. Conf. WEGENER-MEDLAS Project*, Scheveningen.

Spakman, W., 1986. Subduction beneath Eurasia in connection with the Mesozoic Tethys, *Geol. Mijnbouw.*, **65,** 145–153.

Spakman, W. *et al.*, 1988. The Hellenic subduction zone: a tomographic image and its geodynamic implications, *Geophys. Res. Lett.*, **15,** 60–63.

Tselentis, G. A., Stavrakakis, G., Makropoulos, K., Latousakis, J. & Drakopoulos, J., 1988. Seismic moments of earthquakes at the western Hellenic arc and their application to the seismic hazard of the area, *Tectonophysics*, **148,** 73–82.

Valente, J. P., Laj, C., Sorel, D., Roy, S. & Valet, J. P., 1982. Paleomagnetic results from Mio-Pliocene marine series in Crete, *Earth planet. Sci. Lett.*, **57,** 159–172.

APPENDIX

This appendix contains the observed and synthetic seismograms for the earthquakes in this study that were not discussed individually in the main text. The first motion polarity observations for all the events in this study are shown in Fig. 2. For all these events in this appendix except that of 1979 June 15 we carried out tests, of the type described in Figs 4–8 and 10–13, to estimate the uncertainties in strike, dip, rake and centroid depth. These uncertainties, together with the parameters of our minimum misfit solutions, are listed in Table 2. The ISC locations of these events are given in Table 1.

1965 April 9

The waveforms of this event (Fig. A1) confirm that its centroid depth is subcrustal. Reflected phases are clearly identified and require a depth of around 50 km. The minimum misfit depth of 51 km is the same as that estimated from arrival times by the USGS PDE. The ISC estimated a depth of 39 km. The mechanism of this event is tightly constrained by first motion polarities (Fig. 2), with which the minimum misfit solution is compatible. We assumed a water depth of 1.0 km in the source region, but the location of this event close to the southern coast of Crete may have led to the reflection points for *pP*, *sP* and *sS* to some northern stations being on land, rather than underwater. This may explain the anomalous amplitudes of reflected phases at GDH. We suspect that gain at NDI was in fact 3000 on both vertical and horizontal instruments, and not 1500, as marked on the WWSSN film chip. This suspicion comes from comparing the amplitude at NDI with those at QUE and POO, which are close to NDI on the focal sphere. Similarly, by comparing SH at PRE, BUL and NAI, we think the polarities of the long period horizontal instruments at PRE were reversed. In Fig. A1 we have corrected the gain at NDI and the SH polarity at PRE: but in fact, because the stations are weighted azimuthally, these changes made no difference to the inversion.

1966 May 9

First motions (Fig. 2) require this event to be a high-angle reverse fault, but the strike and rake are not well determined by first motions alone. Waveforms (Fig. A2) constrain the centroid depth to 16 +2/−4 km. *SH* polarities at NDI and KOD, and the clearly nodal *SH* arrival at COL are the main constraints on strike (±15°) and rake (±15°). The poor match of the *SH*-waveforms at GDH may imply a change from the normal gain on this instrument: but we could find no direct evidence for this on the WWSSN seismogram station report, and have left it unchanged.

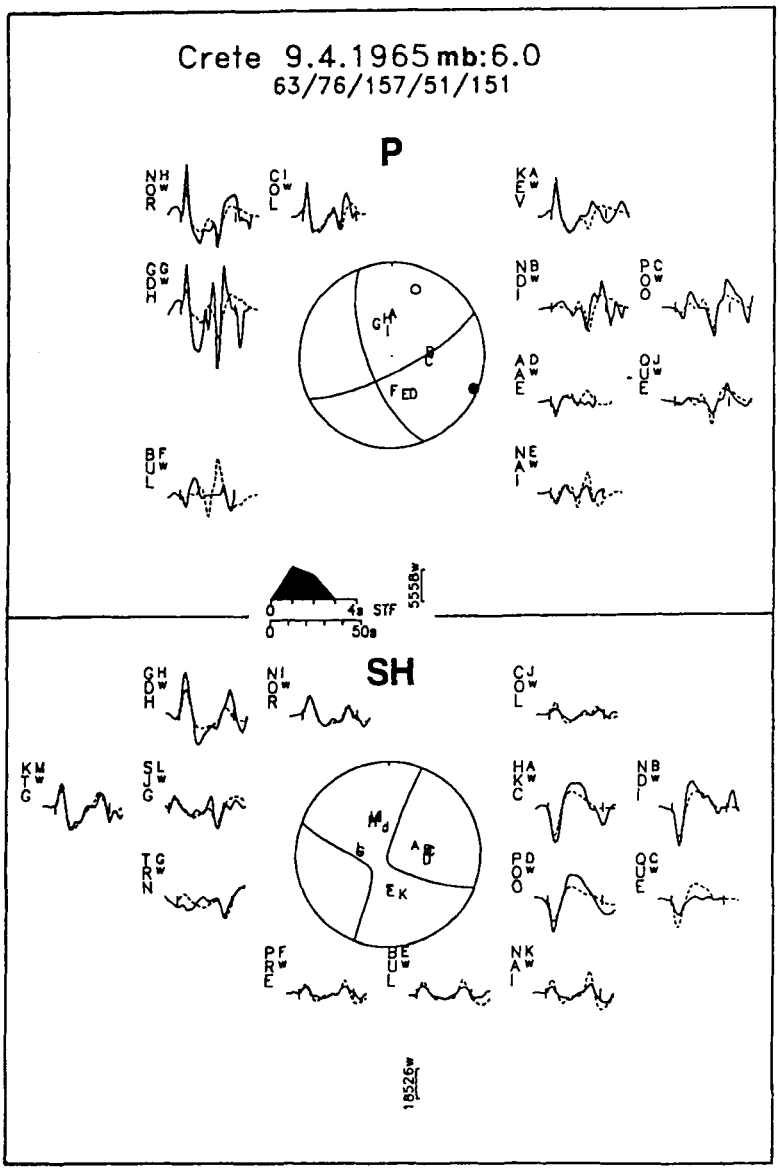

Figure A1. Minimum misfit solution for the earthquake of 1965 April 9. The display convention is that of Fig. 3.

1969 June 12 and 1972 May 4

These events are discussed in the main text (Figs 3–13).

1973 November 29

The first motions for this event (Fig. 2) require a strike–slip component of faulting. The steep nodal plane dipping SW in the minimum misfit solution (Fig. A3a) is compatible with first motions and similar to that in McKenzie's (1978) fault plane solution. McKenzie's (1978) solution shows pure thrust faulting, but with a nodal plane dipping gently NE that is incompatible with the first motions in Fig. 2. We found that we could match the initial parts of the waveforms reasonably well with a source orinetation involving mostly strike–slip motion [Fig. A3(b), row 2]; but with a single source we could not match the prominent peak about 15 s after the first arrival on the *P*-waveforms. This second peak required a second source, or subevent, with an origin time about 15 s after the first. The orientation of the first subevent is constrained reasonably by the first motions and by the changes in *SH* polarity between MAT and POO and between BUL and CAR. We then fixed the parameters of the first subevent and inverted for those of the second: the result is shown in Fig. A3(a) and row 1 of Fig. A3(b). The synthetic waveforms with two subevents match the observed waveforms better than the synthetics involving a single source: but the parameters of the second source are not well resolved. The *P*-waveforms at stations to the east and west require a compressional onset to the second subevent, and its depth is similar to that of the first subevent. We did not attempt to resolve a separation in space between the two subevents. In row 3 of Fig. A3(b) we show waveforms from an inversion in which we fixed the strike, dip and rake to be that of McKenzie's (1978) solution and allowed the depth, time function and moment to be free. The match of *P*-waveforms is not greatly inferior from that in the single shock inversion in row 2, but the match of *SH* at MAT and POO is certainly worse, and this solution is anyway

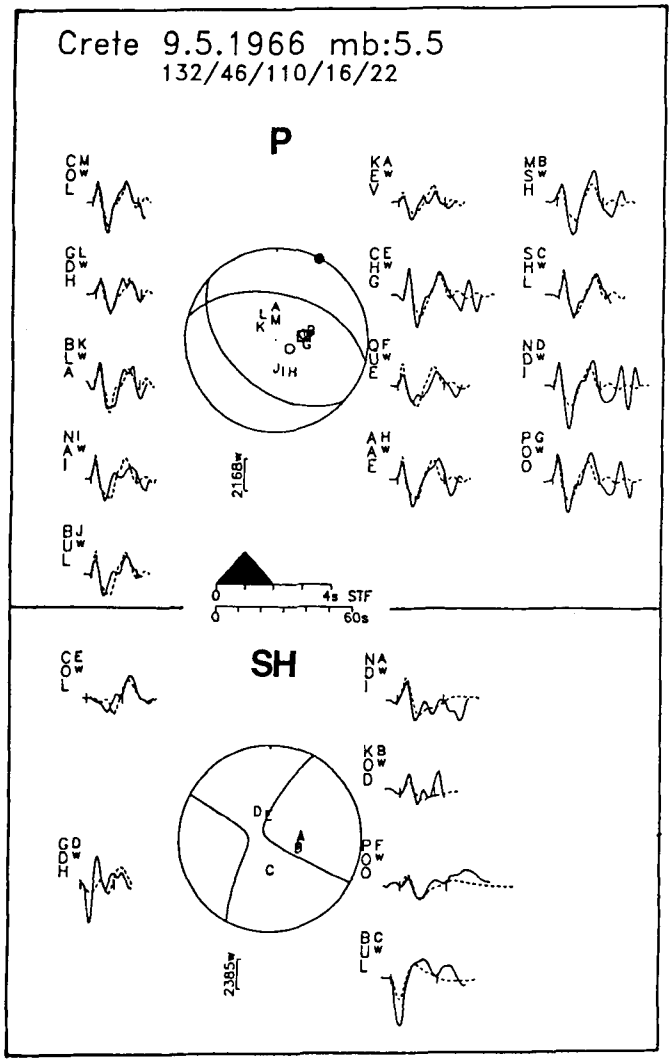

Figure A2. Minimum misfit solution for the earthquake of 1966 May 9. The display convention is that of Fig. 3.

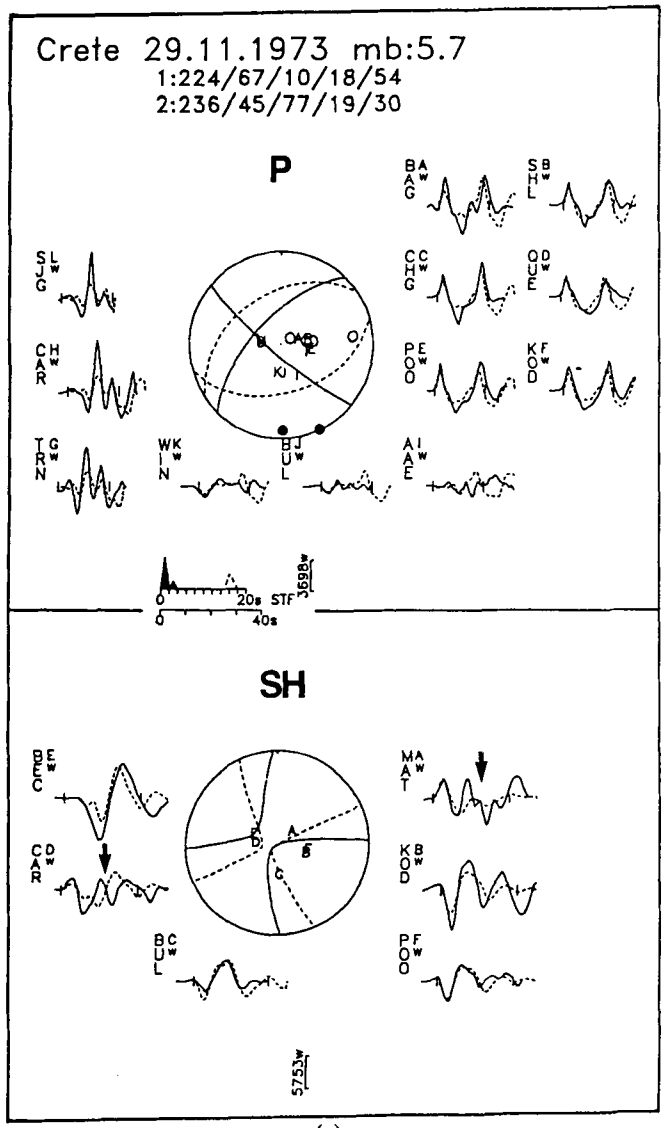

(a)

Figure A3. (a) Minimum misfit solution for the earthquake of 1973 November 29. The display convention is that of Fig. 3. The nodal planes and time function of the postulated second subevent are shown by dashed lines. The strike, dip, rake, depth and moment of the second subevents are shown below those of the first in the header. **(b)** The display convention for this figure is that of Fig. 4. The first row shows the minimum misfit solution of (a) with two subevents. The second row is the first subevent on its own. In the third row the strike, dip and rake were fixed to the values of McKenzie's (1978) first motion solution, while the other parameters were left free.

incompatible with first motions. We were unable to achieve a satisfactory match of amplitudes for *P*-waves at western azimuths (SJG, CAR, TRN), perhaps because this event was located on the SW coast of Crete, with reflection points being on land for some azimuths and under the sea for others.

1975 September 22

This event was clearly deep, with reflected phases easily identifiable on the seismograms (Fig. A4). The minimum misfit depth of 64 km is similar to that of the USGS PDE (63 km) and ISC (55 km). The source orientation is well constrained by first motions and waveforms: the minimum misfit solution is inconsistent with two first motions from nearby stations (Fig. 2), which, however, plot very close to nodal planes, and whose position on the focal sphere must anyway be uncertain, giving the likely velocity heterogeneity in the subducting lithosphere. It is clear, especially from *P*-waveforms, that other phases are present between the direct *P*-waves and the surface reflections. These could be converted or reflected arrivals from structure above the source, but we did not attempt to synthesize them. As in the event of 1965 April 9, it appeared that the gain at NDI should have been 3000 not 1500, and its seismograms have been plotted with this new gain in Fig. A4, though this did not affect the inversion significantly because of the several other stations in almost the same position on the focal sphere.

1977 August 18

The waveforms for this event are shown in Fig. A5. This is one of a group of events, which includes that of 1972 May 4 (Fig. 3), whose waveforms are remarkably similar (Fig. A6). Not surprisingly, the inversion routine returns very similar source orientations and depths for these events. The

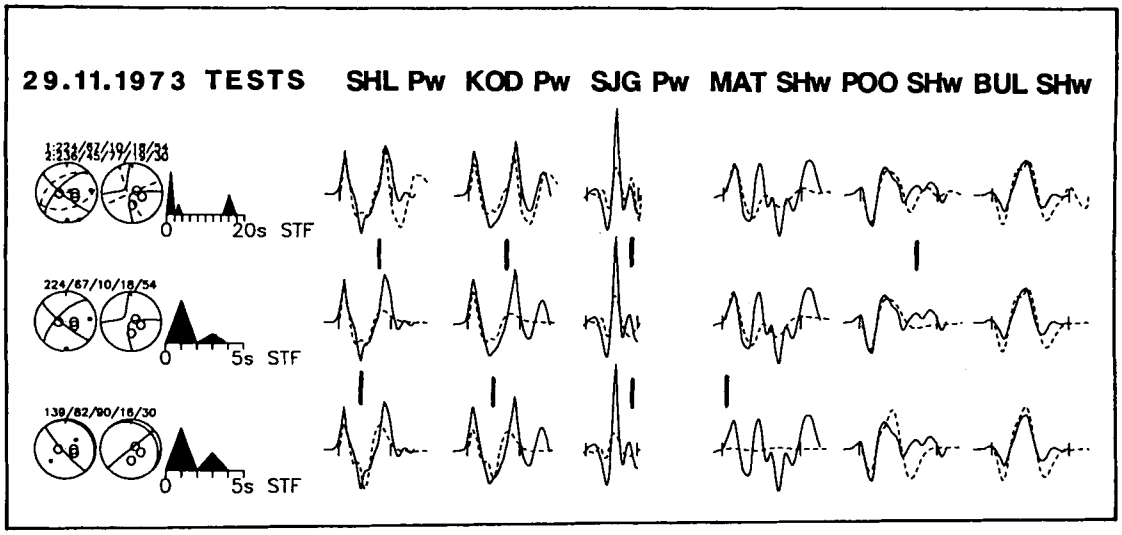

(b)

Figure A3. (*continued*)

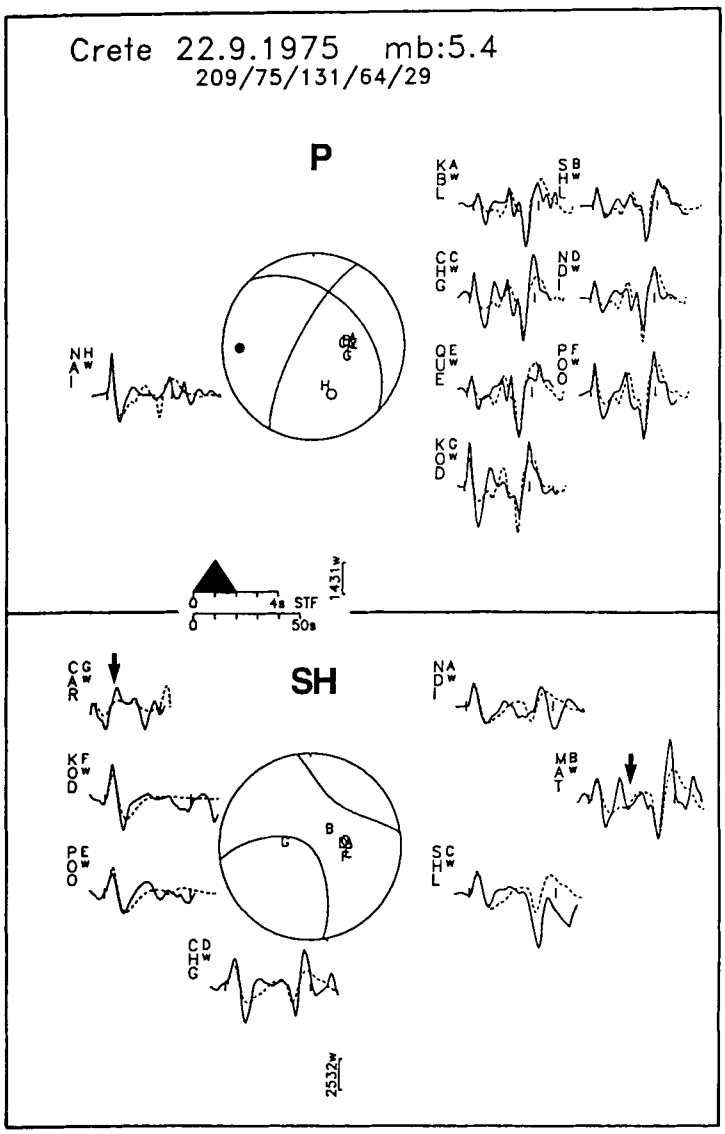

Figure A4. Minimum misfit solution for the earthquake of 1975 September 22. The display convention is that of Fig. 3.

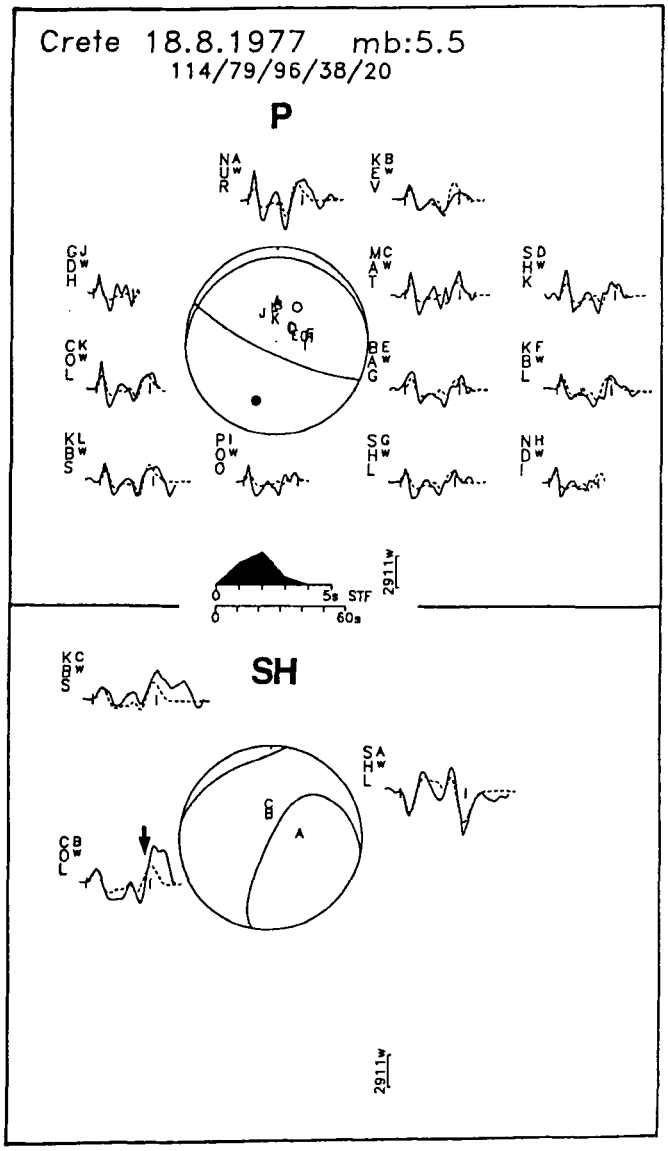

Figure A5. Minimum misfit solution for the earthquake of 1977 August 18. The display convention is that of Fig. 3.

hypocentre of 1977 August 18 is probably within 5 km of that of 1972 May 4, based on relative locations. The fault plane solutions and depths of these events are inferred to be almost identical, within errors, though the seismic moment of the earlier event is about 10 times larger. The uncertainties in source orientation are larger for the 1977 event than for the 1972 one, because of the lack of southern stations: though again the uncertainty is mainly in rake (±20°). Two first motion polarities are inconsistent with the minimum misfit solution, but are close enough to the steep nodal plane to be within the allowable errors in dip. Once again, the gain at NDI appeared to be 3000 rather than 1500, and its seismograms have been plotted with this corrected gain in Fig. A5.

1977 September 11

First motions for this event indicate thrusting, with a dilatation and nodal onsets at northern stations suggesting a relatively steep dip to a nodal plane dipping north. The waveforms for this event (Fig. A7a) are clearly different from the group in Fig. A6: this event is shallower and involves high-angle reverse faulting. An inversion with a single source produces a reasonable fit to *P*-waveforms but not to *SH*: where the prominent second cycle cannot be matched by a single source that is also compatible with the *P*-waves [Fig. A7(b), rows 2 and 4]. The orientation and depth of the first subevent is well constrained by *P*- and *SH*-waves. We then fixed the parameters of this source and inverted for a second source, 11 s after the first. The best solution we obtained involved a strike–slip mechanism for the second subevent (Fig. A7a), and solutions in which the second source was fixed in the same orientation as the first produced inferior matches of seismograms [Fig. A7(b), row 3]. The orientation of the second subevent is not well constrained but must be different from that of the first: its greater effect on *SH*- than on *P*-waveforms is compatible with a mainly strike–slip solution. The depths and moments of the two subevents appear to be similar, and we did not attempt to resolve their spatial separation. Short-period seismograms were clearly recorded for this earthquake. In Fig. A7(c) observed short-period seismograms are compared with synthetics generated for our two sub-event solution. The observed seismograms show energy arriving at the time corresponding to the first arrivals from our inferred second subevent, but this energy is probably mostly from the surface reflections of the first subevent: the contribution of the direct *P* arrivals from the second (strike–slip) subevent is small. As with the events of 1965 April 5, 1975 September 22 and 1977 August 18, the seismograms at NDI are displayed with a gain of 3000, not the 1500 shown on the WWSSN records.

1979 May 15

This is one of the group of events involving thrusting at a depth of about 35–40 km on a shallow plane dipping north (Fig. A6). It occurred about 100 km SE of the other three in Fig. A6, in a region where a different velocity structure at reflection points may have altered details of the waveforms. The solution is well constrained by waveforms and first motions (Figs A8 and 2).

1979 June 15

This is our least satisfactory solution. The first motion polarities (Fig. 2) require a large component of thrusting with a roughly NW strike to one nodal plane. In addition, there are two *SH*-waveforms, at MAT and CHG, the one at MAT having a small, presumably nodal, onset. There were no *P*-waveforms large enough to digitize. Our approach with this earthquake was to see if the first motion and *SH* data indicate whether the mechanism for this event is of the type showing thrusting on E–W planes, or of the type showing reverse faulting on N–S planes. Fig. A9(a) shows short-period *P*- and long-period *SH*-waveforms for the solution we finally adopted. The best constraint on focal depth is from the *SH*-waveform at MAT, though this is complicated by the *ScS* arrival 10 s after direct *S*. If the pulse 20 s after *S* is the surface reflection *sS*, then the depth is around 40 km , and is reasonably well resolved, as seen in

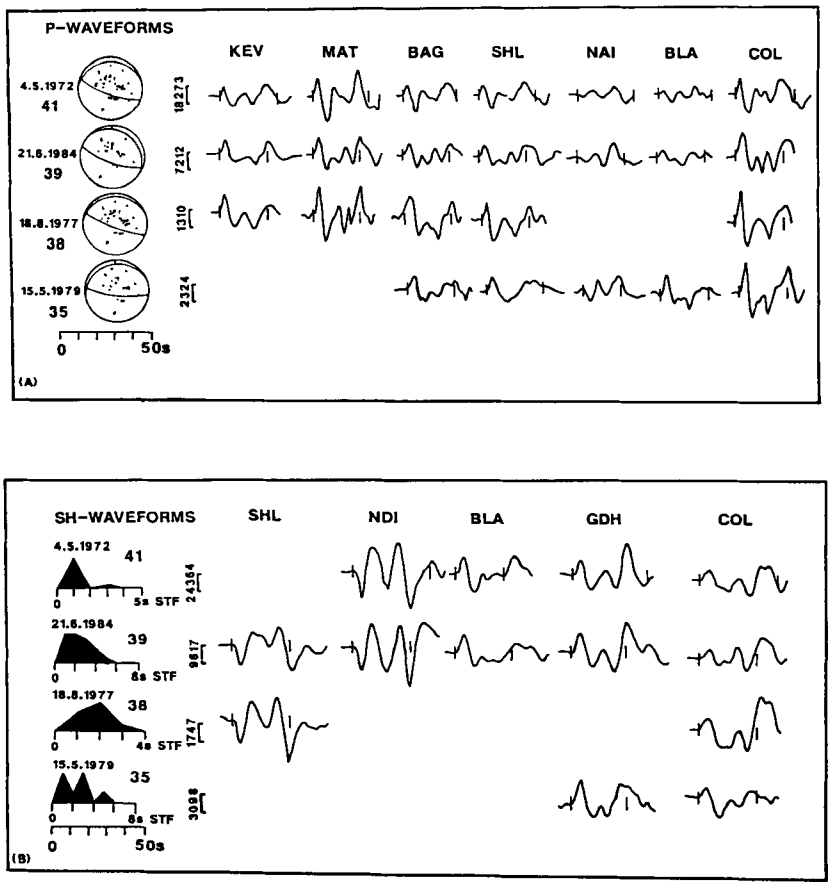

Figure A6. (a) *P*-waveforms and (b) *SH*-waveforms for four earthquakes with similar mechanism and centroid depths. Each row contains the waveforms from the same event. Each column contains waveforms from the same station. Vertical scales are the amplitudes in microns. *P* nodal planes are shown in (a) and time function in (b).

row 2 of Fig. A9(b), where the depth is fixed at 50 km. Although the short-period records at COL, GDH CHG and NDI are unusually clear, they add little positive constraint on focal depth. They are shown in Fig. A9(a) with the synthetic waveforms generated for our adopted solution. In rows 3, 4 and 5 of Fig. A9(a) we have fixed the strike, dip and rake to correspond to low- and high-angle thrusting on E–W planes and reverse faulting on N–S planes respectively. In all three cases the depth was fixed at 40 km, and the time function was free to vary. All three cases show a poor fit to the *SH* waveforms at MAT and CHG, and the mechanisms in rows 3 and 4 are anyway inconsistent with first motions. The adopted solution in row 1 is more consistent with *SH* polarities and waveforms. We conclude, without great confidence, that the focal mechanism was similar to that in Fig. A9(a), which in turn is similar to the better-constrained mechanism of 1983 March 19, at the same latitude 100 km farther east.

1982 August 17

This was one of the larger events in our study, and was well recorded at all azimuths. In occurred on the Mediterranean Rise, 150 km south of Crete, where the crustal structure is enigmatic, but probably involves a greater thickness of sediments than farther north, closer to Crete (Makris & Stobbe 1984). Waveforms suggest that this event occurred in the mantle (Fig. A10a), and, for reasons discussed earlier, we used the same velocity structure as for the other events at similar depths, farther north (Table 1). The mechanism is well constrained by waveforms and the minimum misfit solution is compatible with first motions (Fig. 2). Although *SH* polarities are clear and constrain the solution, the fit to reflected *SH* amplitudes is not good, probably because the reflection coefficients are not well modelled by the simplistic velocity structure we used. In addition, *SH*-waveforms at COL, TATO and HKC are probably contaminated by *ScS*. Our solution is similar to the moment tensor solution obtained by Dziewonski *et al.* (1983b): the difference between the two is within the errors we would anyway estimate for our solution. In Fig. A10(b) we compare waveforms from the two solutions: in the second row we held the orientation fixed at that of Dziewonski *et al.*'s 'best double couple' solution, and inverted for depth, moment and time function. The only significant difference is in the *SH*-waveform at the GDSN station at SCP, which is better matched by our solution.

1983 March 19

The centroid depth of this event is well constrained by clear reflected phases in the *P*-waves at NDI and CHG, and in

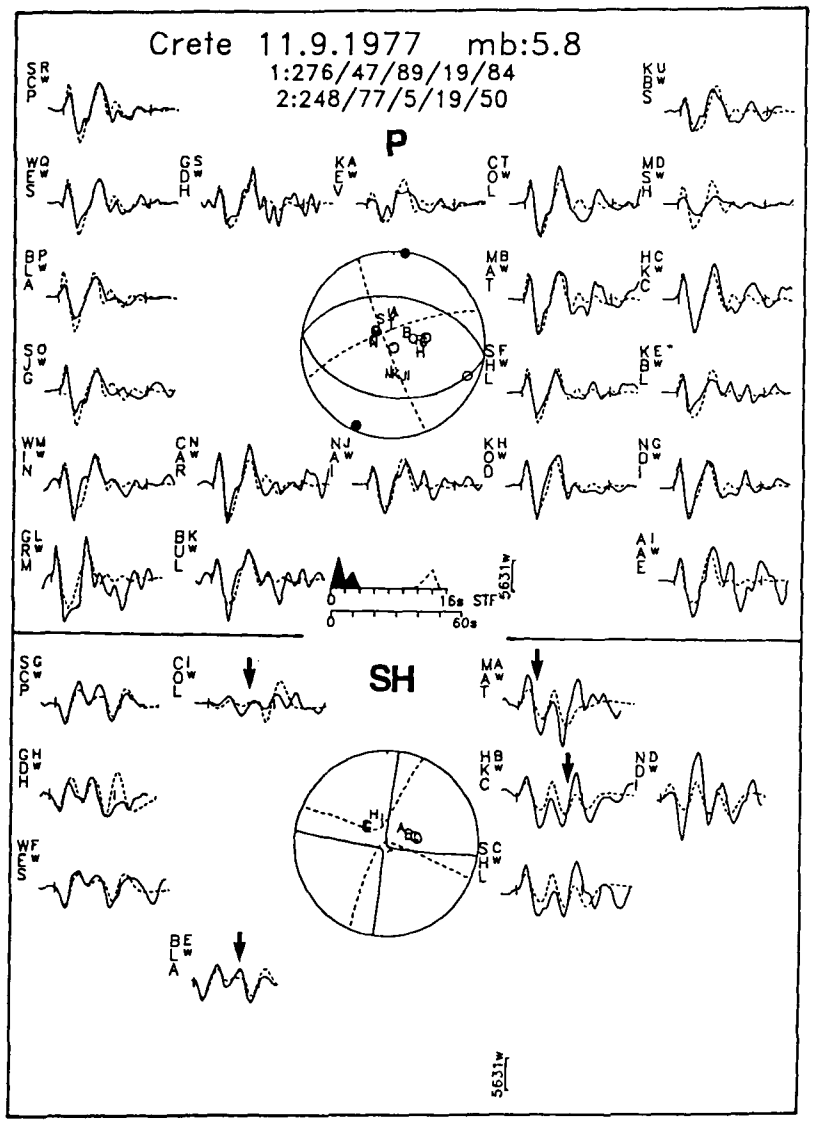

(a)

Figure A7. (a) Minimum misfit solution for the earthquake of 1977 September 11. The display convention is that of Fig. 3. The nodal planes and time function of the postulated second subevent are shown by dashed lines. The strike, dip, rake, depth and moment of the second subevents are shown below those of the first in the header. (b) The display convention for this figure is that of Fig. 4. The first row shows the minimum misfit solution of (a) with two subevents. The second row is the first subevent on its own. The third row shows the results of an inversion in which the second subevent was constrained to have the same orientation and depth as the first. In the fourth row the focal depth for a single subevent was fixed at 35 km in an attempt to match the waveforms with a single source at greater depth. (c) Observed short-period seismograms compared with synthetics generated for the two subevent minimum misfit solution (with $t^* = 0.7$ s for short-period records). Arrows mark the onset of the inferred second subevent.

the *SH*-waves at CAR. The strike, dip and rake are also well resolved, and the minimum misfit solution is compatible with the first motion polarities (Fig. 2), which themselves tightly constrain the nodal plane dipping W. The 'best double couple' mechanism found by the moment tensor inversion of Dziewonski, Friedman & Woodhouse (1983a) is similar to ours, but rotated 45° anticlockwise. In row 2 of Fig. A11(b) we fixed the strike, dip and rake to that of Dziewonski *et al.*'s solution, leaving the depth and time function free to change. The resulting waveforms can be compared with those of our minimum misfit solution (row 1). Dziewonski *et al.*'s solution produces an inferior fit to SH at NDI, and also violates some first motions at western stations.

1984 June 21

This is another event in the group at the SW corner of Crete, all of which have similar waveforms and mechanisms (Fig. A6). The constraints and uncertainties in the source parameters of this event are similar to those of 1972 May 4 (Figs 3–8) and 1977 August 18 (Fig. A5). The moment tensor solution of Dziewonski, Franzen & Woodhouse (1985) is similar to our minimum misfit solution, but has the steep (presumably auxiliary) nodal plane dipping 85°NE instead of 72°SW. A comparison of the waveforms from the two solutions is shown in Fig. A12(b), in which we fixed the source orientation to that of Dziewonski *et al.*'s (1985) solution, and inverted for depth, moment and source time

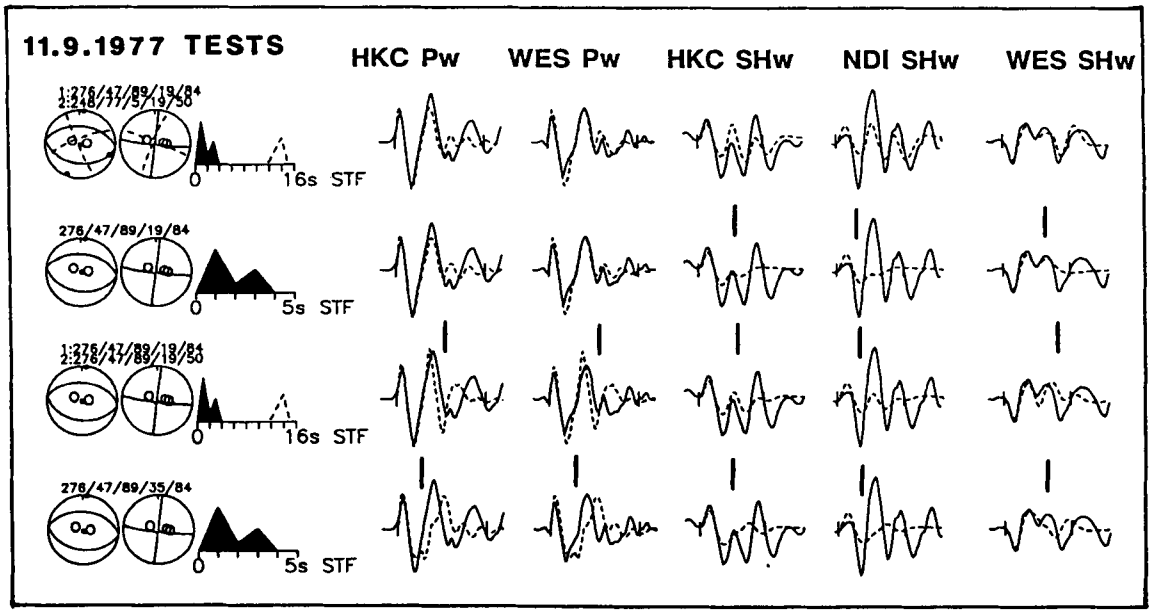

(b)

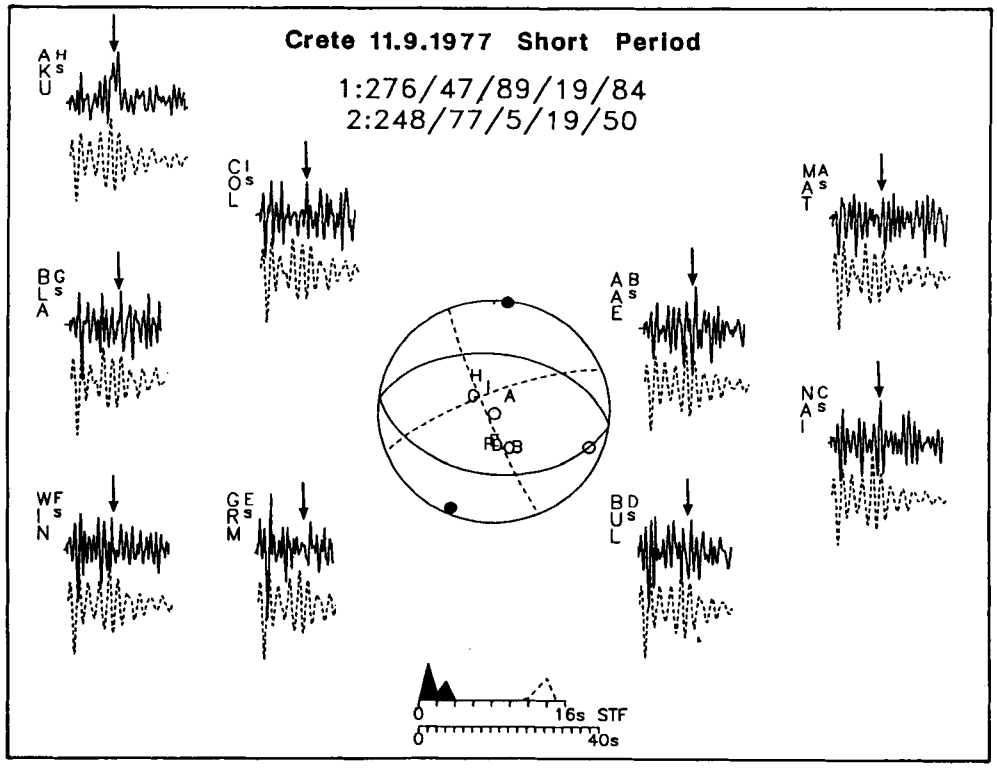

(c)

Figure A7. (*continued*)

function. The match between observed and synthetic waveforms is better, particularly for *P*-waves, in our minimum misfit solution: implying that the shallow dipping nodal plane dips gently NE rather than SW. Once again, we suspect the true gain at NDI was 3000 not 1500, and have plotted its waveforms with this revised gain. As before, the effect of this change on the inversion was negligible.

1985 September 27

In spite of the paucity of waveforms available for this event (Fig. A13a), its focal parameters are surprisingly well determined. The focal depth is constrained by the clear reflected phase visible on the *SH* record at GDH. In row 2 of Fig. A13(b) the depth has been perturbed by 8 km with

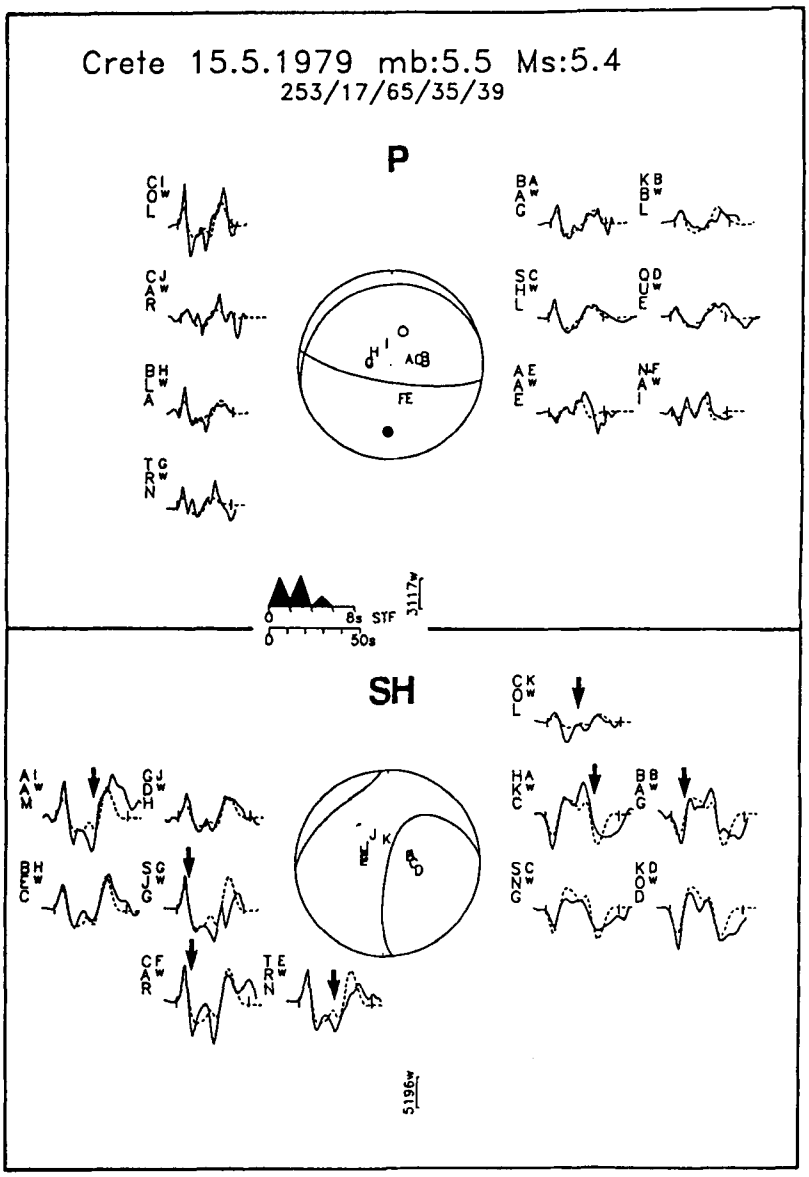

Figure A8. Minimum misfit solution for the earthquake of 1979 May 15. The display convention is that of Fig. 3.

the other parameters left free: the *SH* fit at GDH is noticeably worse. The strike is well constrained by the nodal position of the *SH*-waveforms at GDH and CHG: as seen in row 3 of Fig. A13(b), where the strike has been perturbed by 15°, while the other parameters are left free. The same stations constrain the dip, which, when perturbed by 13° (row 4 of Fig. A13b) leads to a worse fit for *P* and *SH* at CDH and for *SH* at CHG. A change in rake of 9° (row 5 in Fig. A13b) affects the amplitudes of *P* at GDH and NUR and of *SH* at GDH. Note that, when one parameter is perturbed and then fixed, the values returned for the other parameters do not differ much from those of the minimum misfit solution. As a result of many tests of the type shown in Fig. A13(b), we are able to estimate the errors in our minimum misfit solution as: strike ±10°; dip ±10°; rake +10°/−5°, depth ±4 km. The best double couple solution of Dziewonski *et al.*'s (1986) moment tensor inversion is very similar to our minimum misfit solution, the main difference being a 10° change in strike. This is at the limit of our acceptable errors, but even this change produces a worse fit to *SH* amplitudes when the strike, dip and rake are fixed and the other parameters are left free (Fig. A13b, row 6). This is an important earthquake in our study as it clearly has a very different mechanism and depth from that of 1966 May 9, which had virtually the same epicentre.

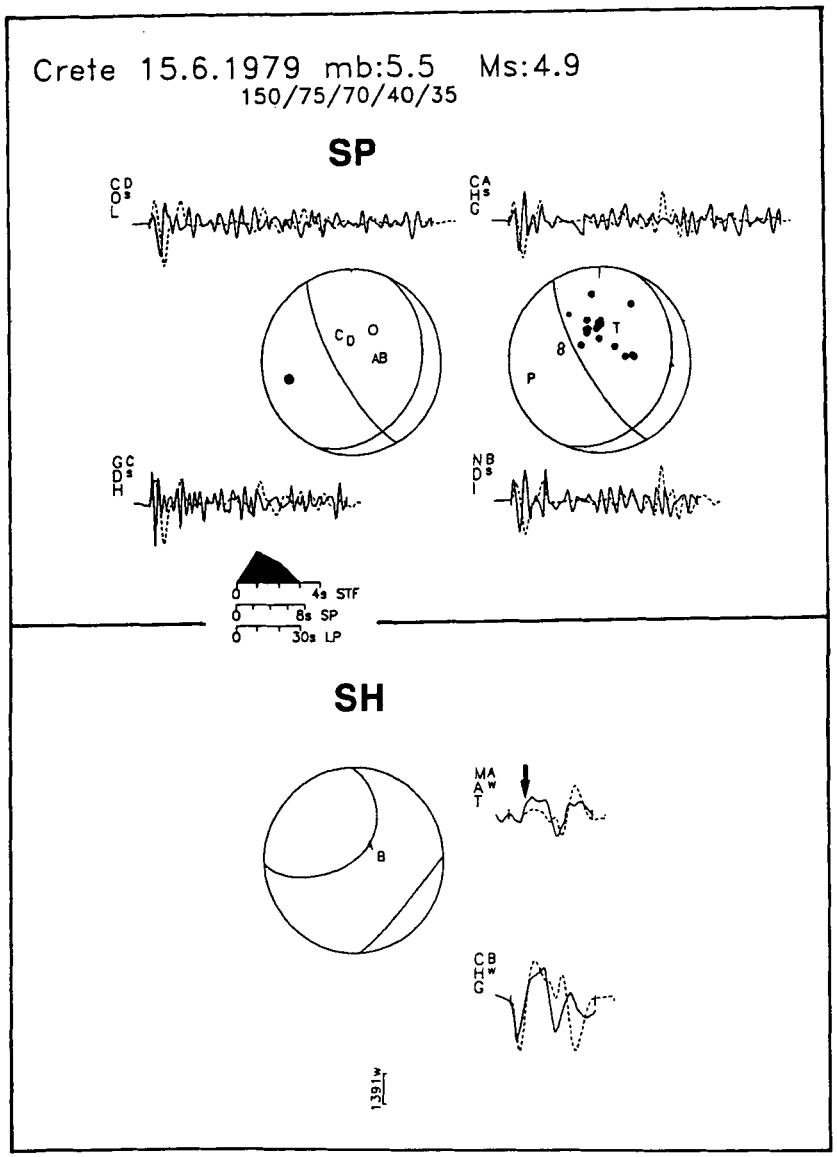

(a)

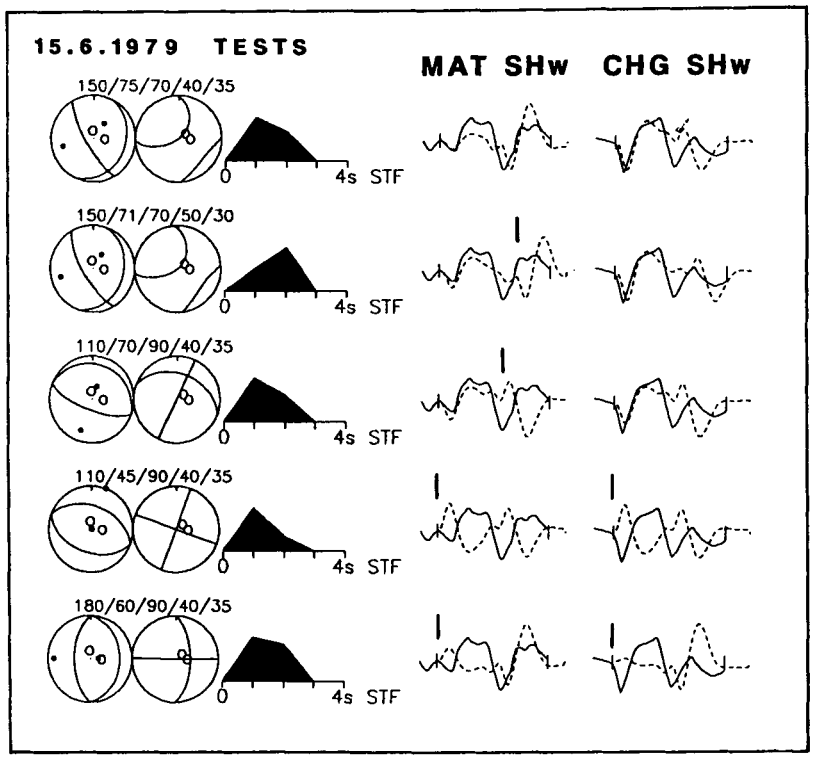

(b)

Figure A9. (a) Short-period (top) and long-period *SH* (bottom) waveforms for our adopted solution for the earthquake of 1979 June 15. The display convention is that of Fig. 3, with a focal sphere showing first motion polarities added. (b) This figure follows the convention of Fig. 4. *SH*-waveforms at MAT and CHG are shown for our adopted solution in the top row. In row 2 the focal depth was fixed at 50 km. In rows 3–5 the strike, dip and rake were fixed to resemble the mechanism of events in groups (b), (c) and (d).

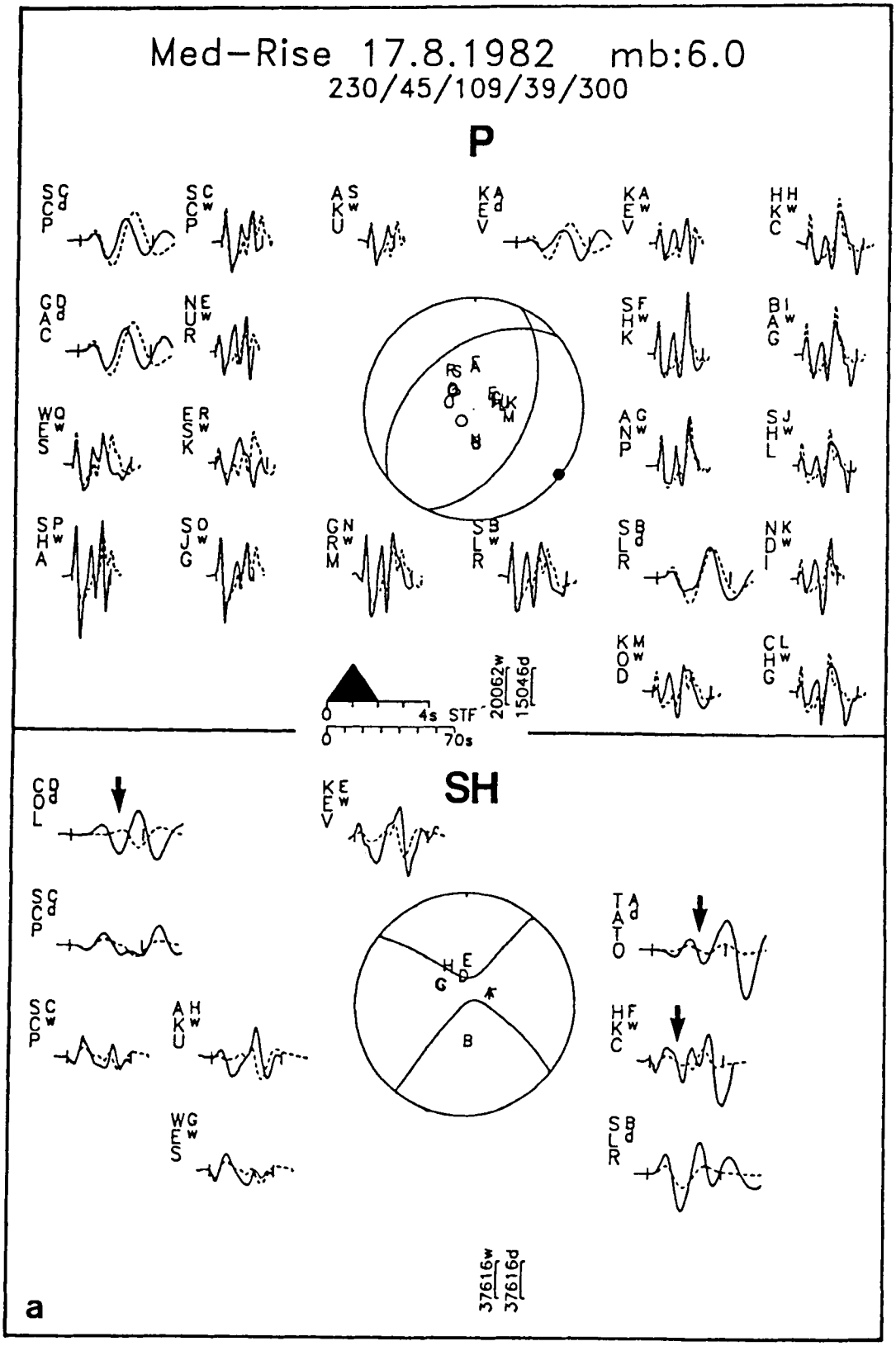

Figure A10. (a) Minimum misfit solution for the earthquake of 1982 August 17. The display convention is that of Fig. 3. (b) Selected waveforms of our minimum misfit solution (row 1) are compared with those generated by an inversion in which the strike, dip and rake were fixed to the values of Dziewonski *et al.*'s (1983b) best double couple solution (row 2). The format is that of Fig. 4.

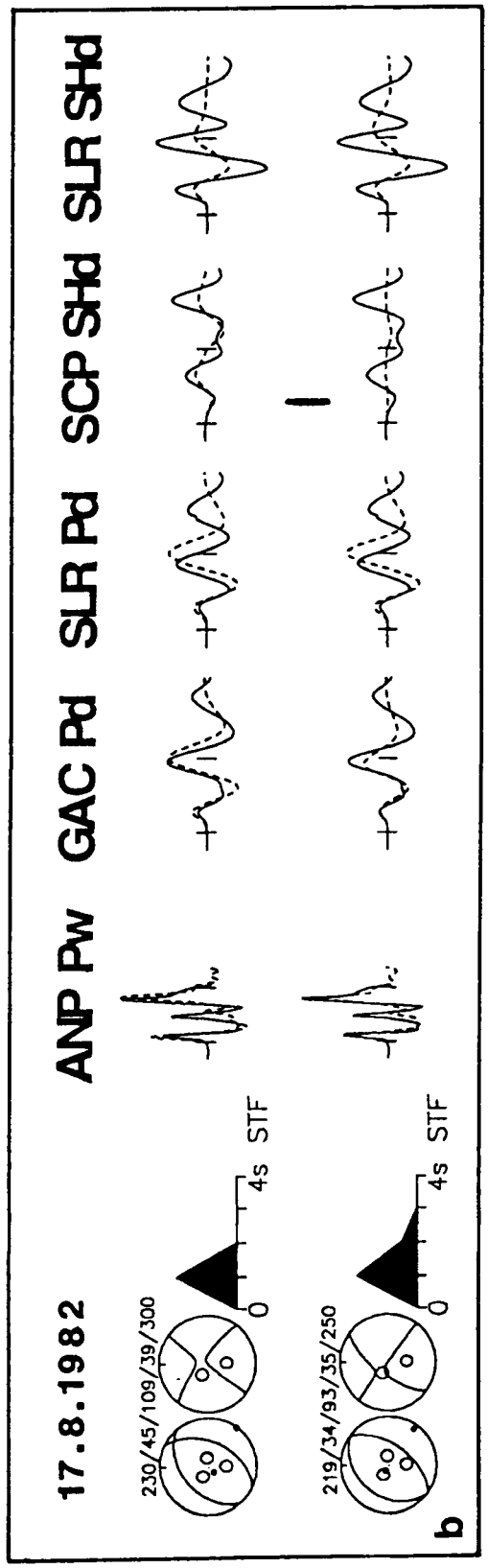

Figure A10. (*continued*)

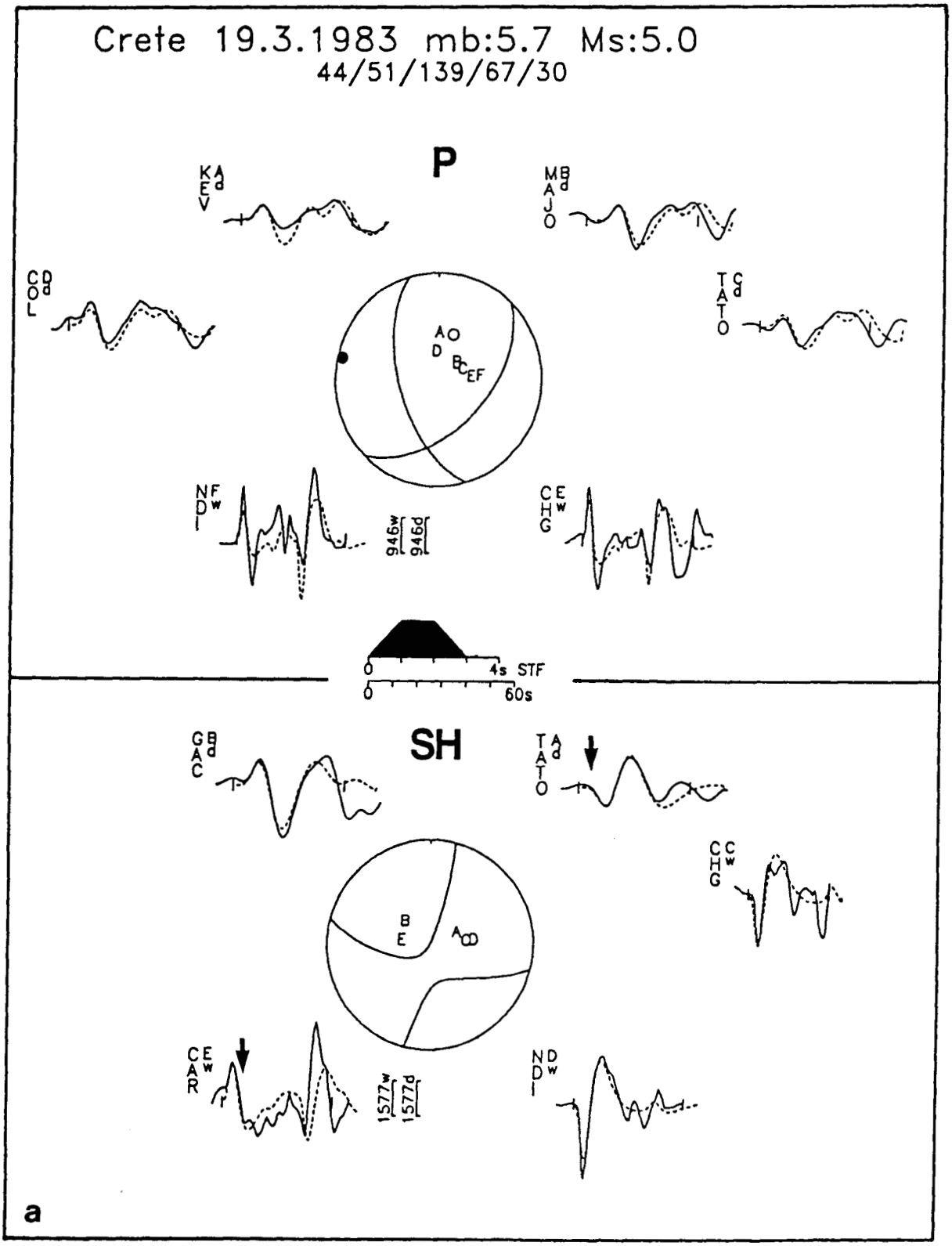

Figure A11. (a) Minimum misfit solution for the earthquake of 1983 March 19. The display convention is that of Fig. 3. (b) Selected waveforms of our minimum misfit solution (row 1) are compared with those generated by an inversion in which the strike, dip and rake were fixed to the values of Dziewonski *et al.*'s (1983a) best double couple solution (row 2). The format is that of Fig. 4.

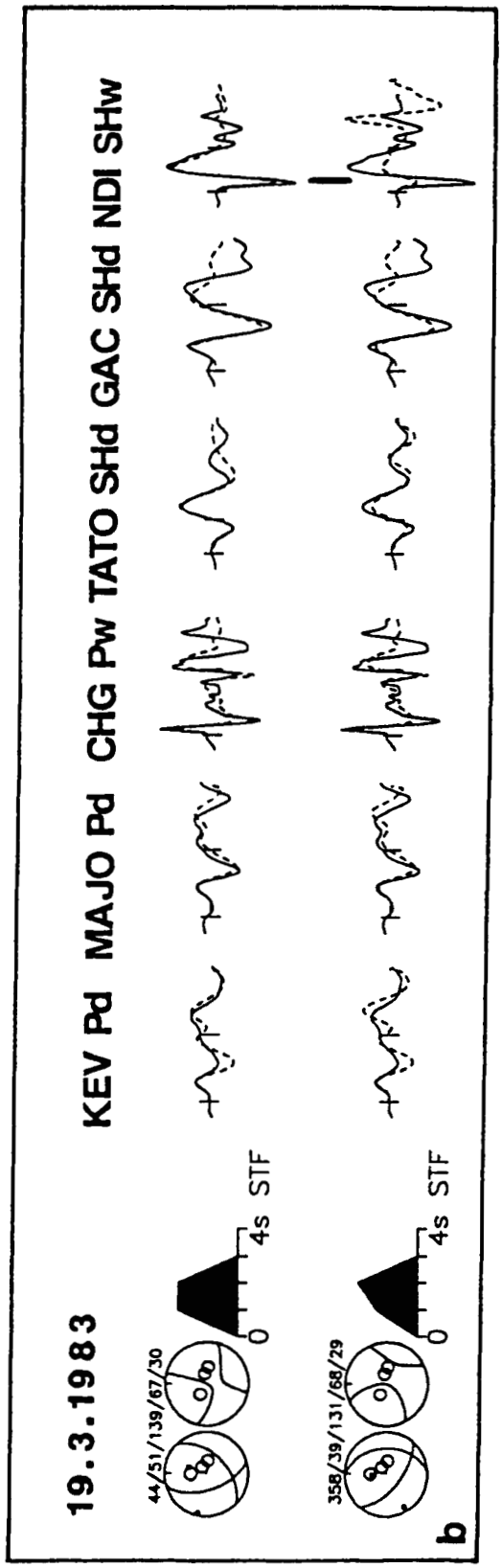

Figure A11. (*continued*)

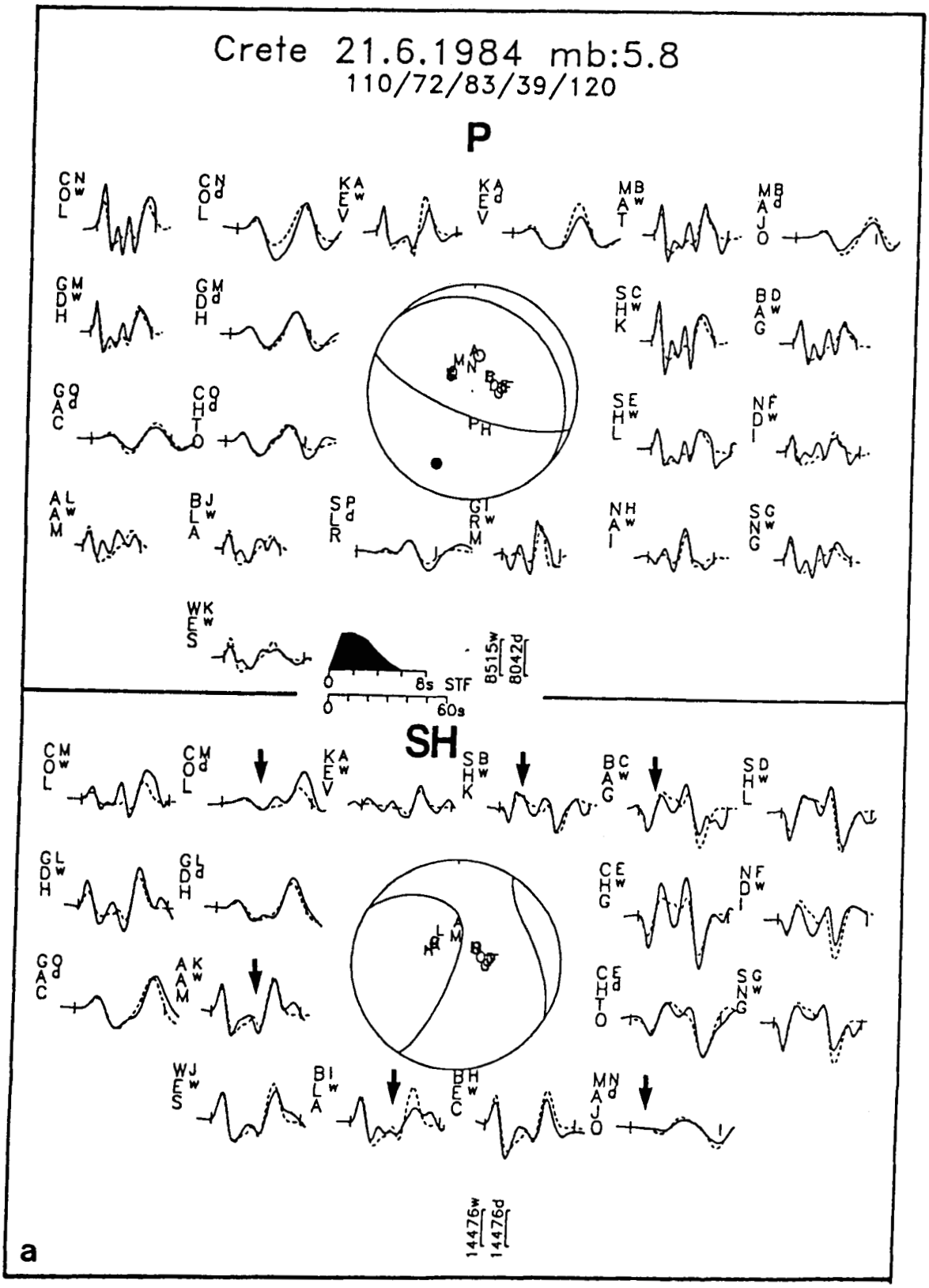

Figure A12. (a) Minimum misfit solution for the earthquake of 1984 June 21. The display convention is that of Fig. 3. (b) Selected waveforms of our minimum misfit solution (row 1) are compared with those generated by an inversion in which the strike, dip and rake were fixed to the values of Dziewonski *et al.*'s (1985) best double couple solution (row 2). The format is that of Fig. 4.

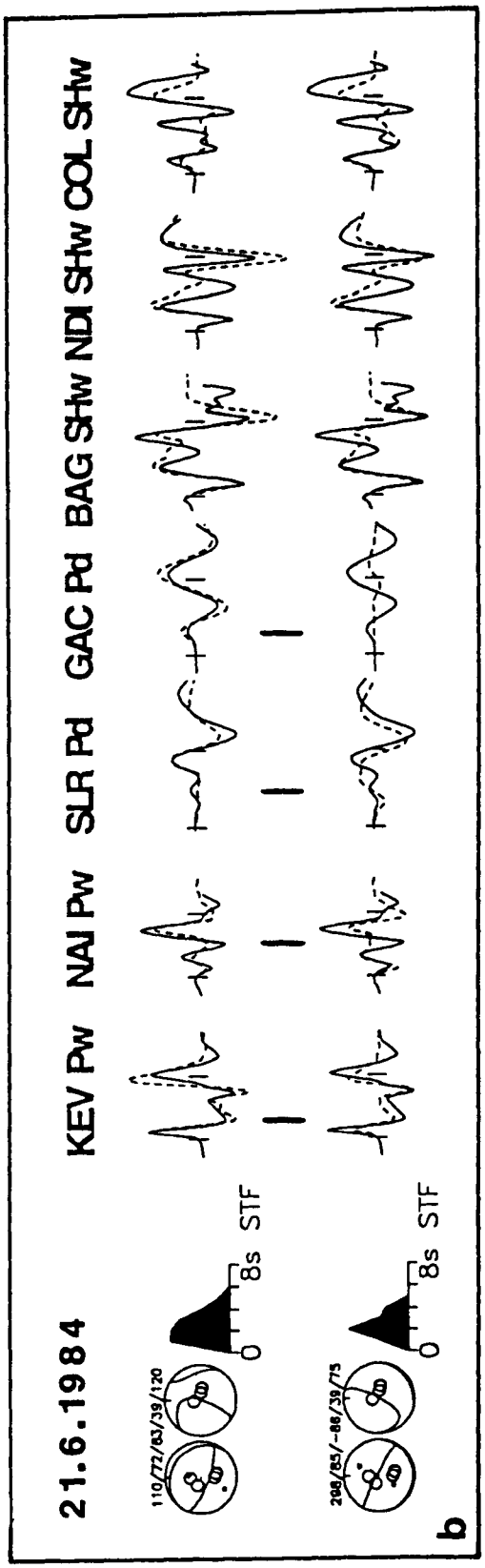

Figure A12. (*continued*)

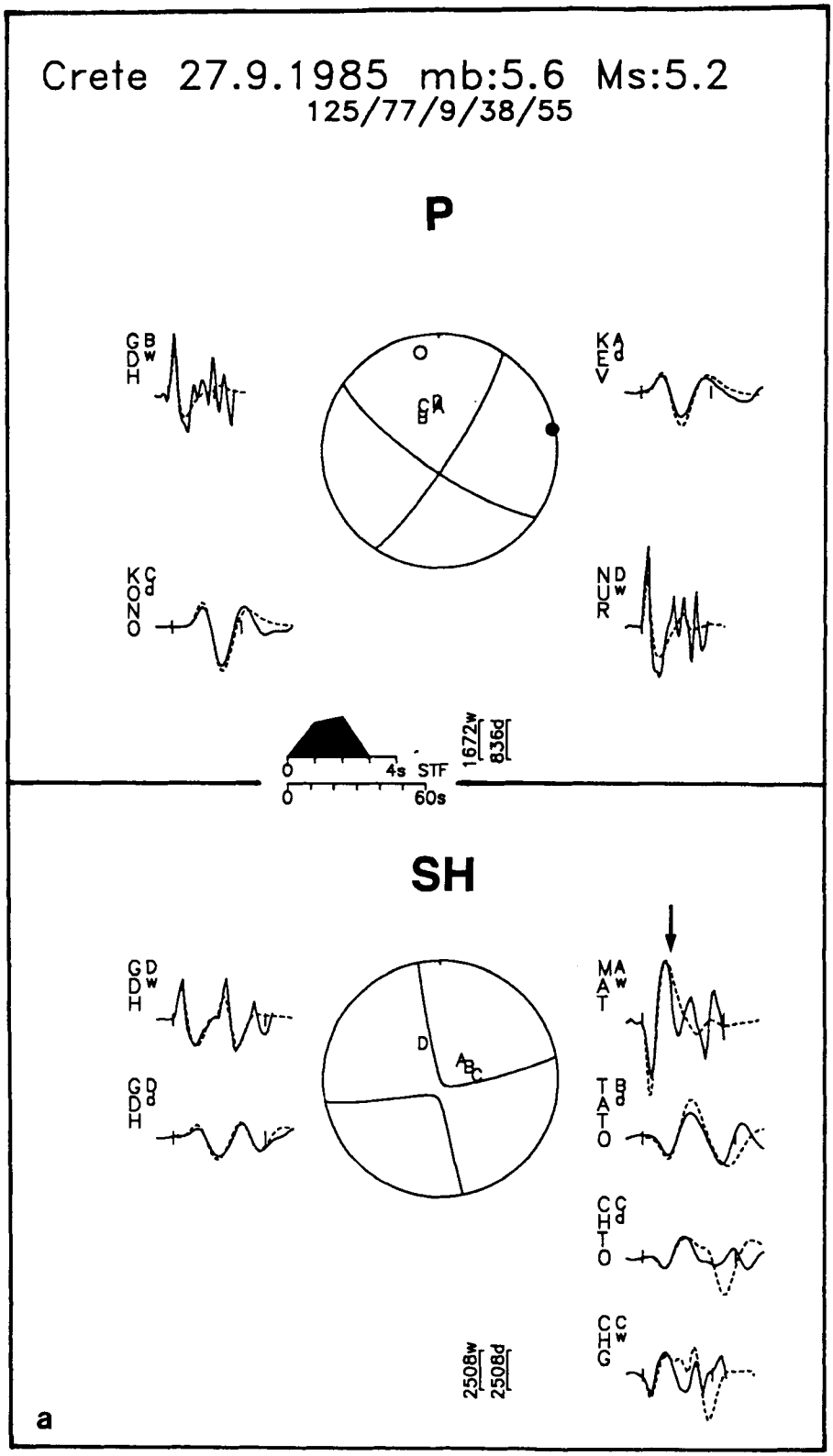

Figure A13. (a) Minimum misfit solution for the earthquake of 1985 September 27. The display convention is that of Fig. 3. (b) This figure is in the format of Fig. 4. In the top row is the minimum misfit solution. In rows 2–5 one parameter is fixed and the rest are left free. The depth, strike, dip and rake are fixed in rows 2–5 respectively. In row 6, the strike, dip and rake were fixed to the values of Dziewonski *et al.*'s (1986) best double couple solution, with the depth and time function left free.

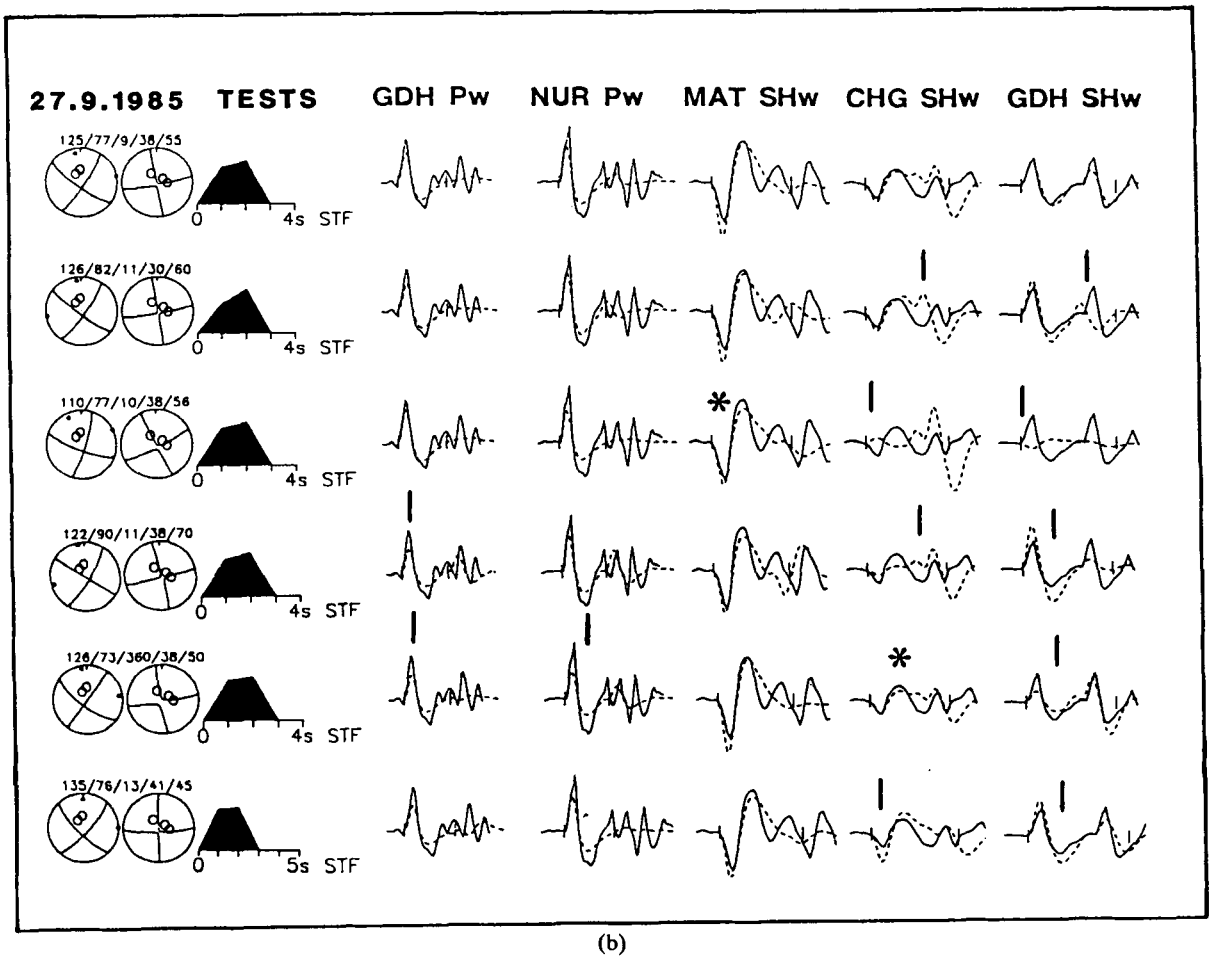

(b)

Figure A13. (*continued*)